The Plant Cell, Vol. 29: 1726–1747, July 2017, www.plantcell.org © 2017 The author(s).

Suppressors of the Chloroplast Protein Import Mutant *tic40* Reveal a Genetic Link between Protein Import and Thylakoid Biogenesis

Jocelyn Bédard,[a,b,1] Raphael Trösch,[b,1,2] Feijie Wu,[b,3] Qihua Ling,[a,b] Úrsula Flores-Pérez,[a,b] Mats Töpel,[b,4] Fahim Nawaz,[a,5] and Paul Jarvis[a,b,6]

[a] Department of Plant Sciences, University of Oxford, Oxford OX1 3RB, United Kingdom
[b] Department of Biology, University of Leicester, Leicester LE1 7RH, United Kingdom

ORCID IDs: 0000-0003-3204-0122 (J.B.); 0000-0002-0632-3324 (R.T.); 0000-0002-5016-3460 (F.W.); 0000-0002-6984-9921 (Q.L.); 0000-0002-6780-3671 (Ú.F.-P.); 0000-0001-7989-696X (M.T.); 0000-0001-7753-5087 (F.N.); 0000-0003-2127-5671 (P.J.)

To extend our understanding of chloroplast protein import and the role played by the import machinery component Tic40, we performed a genetic screen for suppressors of chlorotic *tic40* knockout mutant *Arabidopsis thaliana* plants. As a result, two *suppressor of tic40* loci, *stic1* and *stic2*, were identified and characterized. The *stic1* locus corresponds to the gene *ALBINO4* (*ALB4*), which encodes a paralog of the well-known thylakoid protein targeting factor ALB3. The *stic2* locus identified a previously unknown stromal protein that interacts physically with both ALB4 and ALB3. Genetic studies showed that ALB4 and STIC2 act together in a common pathway that also involves cpSRP54 and cpFtsY. Thus, we conclude that ALB4 and STIC2 both participate in thylakoid protein targeting, potentially for a specific subset of thylakoidal proteins, and that this targeting pathway becomes disadvantageous to the plant in the absence of Tic40. As the *stic1* and *stic2* mutants both suppressed *tic40* specifically (other TIC-related mutants were not suppressed), we hypothesize that Tic40 is a multifunctional protein that, in addition to its originally described role in protein import, is able to influence downstream processes leading to thylakoid biogenesis.

INTRODUCTION

Plastids are plant cell organelles that each form an enclosed compartment containing ~3000 different protein species, depending on the developmental stage and tissue-specific differentiation (Sun et al., 2004; Leister, 2016). While a small fraction of plastid proteins are encoded on the plastid genome, most are encoded on the nuclear genome as preproteins with an N-terminal transit peptide and imported posttranslationally through the translocons at the outer (TOC) and inner (TIC) chloroplast envelope membranes (Jarvis, 2008; Li and Chiu, 2010; Shi and Theg, 2013; Demarsy et al., 2014; Paila et al., 2015). Plastid targeting specificity is conferred by the Toc34 and Toc159 families of TOC receptors in the outer plastid membrane, which can specifically interact with the transit peptides of preproteins. Each preprotein is then threaded through adjacent TOC and TIC channels in the outer and inner envelope membranes. The transit peptide is cleaved off by the stromal processing peptidase when the preprotein emerges on the stromal side of the channel, and the mature protein then either is folded to its native structure or engages downstream targeting pathways (Jarvis, 2008; Li and Chiu, 2010; Shi and Theg, 2013; Demarsy et al., 2014; Paila et al., 2015).

The identity and nature of the TIC channel is disputed and subject to current research. Suggested TIC channel subunits are Tic110 (Heins et al., 2002), Tic20 (Chen et al., 2002), and Tic21 (Teng et al., 2006). The C terminus of Tic110 has been reported to form either four transmembrane domains (Heins et al., 2002; Balsera et al., 2009) or a stromal scaffold for chaperone binding (Jackson et al., 1998; Inaba et al., 2003, 2005). A recent detailed structural analysis of Tic110 supports the latter model (Tsai et al., 2013), which makes a channel function for Tic110 structurally unlikely. However, the severe embryo-lethal phenotype of *Arabidopsis thaliana tic110* mutants and the proposed association of Tic110 with TOC proteins (Akita et al., 1997; Kovacheva et al., 2005) suggest an essential role of Tic110 in the late steps of protein import, e.g., in import propulsion, precursor processing or folding, or postimport inner membrane insertion. Recently, a 1 MD complex that associates with translocation intermediate precursor proteins was isolated from inner envelope membranes and found to comprise three novel components, Tic214, Tic100, and Tic56, as well as Tic20 and Tic21 (Kikuchi et al., 2013). Knockout mutants of all these components have severe phenotypes (Chen et al., 2002; Teng et al., 2006; Kikuchi et al., 2013); thus, the 1 MD complex seems to play an essential role in protein import.

[1] These authors contributed equally to this work.
[2] Current address: University of Kaiserslautern, Department of Biology, Erwin-Schrödinger-Strasse 70, DE-67663 Kaiserslautern, Germany.
[3] Current address: Shanghai Institute of Plant Physiology and Ecology (SIPPE), 319 Yueyang Road, Xuhui District, Shanghai 200031, China.
[4] Current address: Department of Marine Sciences, University of Gothenburg, Box 460, SE-40530 Göteborg, Sweden.
[5] Current address: Department of Agronomy, MNS University of Agriculture, Multan, Pakistan.
[6] Address correspondence to paul.jarvis@plants.ox.ac.uk.
The author responsible for distribution of materials integral to the findings presented in this article in accordance with the policy described in the Instructions for Authors (www.plantcell.org) is: Paul Jarvis (paul.jarvis@plants.ox.ac.uk).

www.plantcell.org/cgi/doi/10.1105/tpc.16.00962

Importantly, Tic110 is not part of the 1 MD complex (Kikuchi et al., 2013). Instead, it interacts with Tic40 and the stromal chaperone Hsp93, which have been suggested to form a motor complex (Chou et al., 2003, 2006). Tic40 is anchored in the inner membrane by a single N-terminal transmembrane domain, while its stromal C terminus comprises a putative tetratricopeptide repeat (TPR) domain and a domain also found in the Hsp70-interacting protein (Hip) and Hsp70/Hsp90-organizing protein (Hop) cochaperones (Chou et al., 2003, 2006; Bédard et al., 2007; Kao et al., 2012). Interaction of Tic40 with Tic110 via its TPR domain may release preproteins from Tic110 to enable precursor processing, whereas the Tic40 Hip/Hop domain may stimulate the ATPase activity of Hsp93, possibly to provide a driving force for the import process (Chou et al., 2006). However, it was recently suggested that this energy is not used for protein import per se, but rather for quality control (Sjögren et al., 2014; Flores-Pérez et al., 2016) and/or precursor processing (Huang et al., 2016). Instead, plastid-localized cpHsp70 may be the dominant player in protein import propulsion (Su and Li, 2010; Liu et al., 2014; Huang et al., 2016).

Once a preprotein reaches the stromal side of the chloroplast envelope and its transit peptide has been cleaved off by the stromal processing peptidase, in many cases, the protein is further targeted to its correct subcompartment within the chloroplast. For example, some proteins are reinserted into the inner envelope membrane after first being released into the soluble stromal phase (Tripp et al., 2007; Chiu and Li, 2008; Viana et al., 2010). Other imported proteins, mainly those involved in the photosynthetic electron transfer reactions, are targeted via different pathways to the thylakoids (Celedon and Cline, 2013). Thylakoid lumen proteins usually carry further targeting information at their N-terminal ends, which directs their targeting via the chloroplast secretory (cpSec) pathway or the chloroplast twin arginine translocation (cpTat) pathway. Thylakoid membrane proteins may insert spontaneously, use one of the aforementioned pathways, or engage the chloroplast signal recognition particle (cpSRP) pathway (the latter is employed predominantly by light-harvesting chlorophyll binding proteins [LHCPs]) (Celedon and Cline, 2013).

In the cpSRP transport pathway, LHCP proteins are recognized by a bipartite cpSRP composed of cpSRP54, an ortholog of the bacterial SRP protein, and cpSRP43, a protein that specifically recognizes a targeting signal within LHCP termed L18 (Schuenemann et al., 1998; Tu et al., 2000; Stengel et al., 2008). The cpSRP cooperates in a GTP-dependent manner with cpFtsY, an ortholog of the SRP receptor, to deliver LHCP to ALBINO3 (ALB3), an ortholog of the bacterial YidC protein and a member of the Alb3/Oxa1/YidC insertase family. The ALB3 protein then mediates the insertion (and assembly) of the LHCP protein into the thylakoid membrane (Moore et al., 2000; Falk et al., 2010; Dünschede et al., 2011). Accordingly, Arabidopsis *alb3* mutants display a strongly chlorotic/albino phenotype linked to defective LHCP biogenesis (Sundberg et al., 1997; Asakura et al., 2008); by contrast, those with defects affecting a second, paralogous protein called ALB4 appear relatively normal, suggesting that this factor is functionally different (Gerdes et al., 2006; Benz et al., 2009; Trösch et al., 2015). Recently, a novel component of the cpSRP pathway was identified: The LHCP targeting deficient (LTD) protein acts upstream of the cpSRP by mediating the transfer of the newly imported LHCP proteins from the TIC translocon to the cpSRP complex (Ouyang et al., 2011). Interestingly, Tic40 and Tic110 were both implicated in LTD association with the TIC, and in early recognition of LHCPs (Ouyang et al., 2011). Thus, Tic40 may have an additional role in the onward targeting of some thylakoid proteins, which is possibly analogous to its proposed function in the postimport reinsertion of other proteins into the inner envelope membrane (Chiu and Li, 2008).

More work is needed to clarify the role of Tic40 in chloroplast protein transport. Because Tic40 is encoded in Arabidopsis by a single gene that upon mutation causes a distinct yet viable chlorotic phenotype (Chou et al., 2003; Kovacheva et al., 2005), it is well suited for analysis using a forward-genetic suppressor screen. Here, we describe such a screen, along with the detailed characterization of the resulting *stic1* and *stic2* suppressor mutants.

RESULTS

Identification of *suppressor of tic40* Mutants

To identify mutant plants in which the chloroplast protein import defect displayed by *tic40* is suppressed, ~40,000 *tic40-4* seeds were mutagenized using EMS. The M1 plants were grown to maturity to produce the M2 generation of seeds, and the progeny of ~10,000 M1 plants was screened for putative *suppressor of tic40* (*stic*) mutants. Because young *tic40* seedlings display a reduced size and clear pale-green mutant phenotype (Chou et al., 2003; Kovacheva et al., 2005), it was assumed that suppression of *tic40* would result in improved growth and a darker green phenotype. Thus, M2 seeds were germinated and grown in vitro for 10 d and then screened visually for seedlings that appeared significantly larger and greener than the *tic40*-like seedlings. This led to the identification of several putative *stic* mutants, which were thoroughly characterized genetically to exclude false positives, and further backcrossed to *tic40-4* to remove unwanted background mutations.

A subset of seven mutants carrying mutations that were transmitted in a Mendelian fashion were selected for further characterization and for identification of the mutations responsible for the suppression effect. The selected *stic* mutants suppressed the *tic40* mutation to a similar degree, as they had comparable phenotypes (Figures 1A and 1B). Moreover, all were found to be semidominant: The F1 progeny from their backcrosses to *tic40* displayed phenotypes that were intermediate between *tic40* single mutants and *stic tic40* double homozygotes (Supplemental Figure 1), while the F2 progeny from these crosses segregated in a 1:2:1 ratio for *tic40*-like, intermediate, and full-suppressor-type plants, respectively. Rough mapping of the mutations (see "Molecular Identification of the *stic1* and *stic2* Loci" section below) revealed that they fall into two allelic groups, identifying two loci, with five mutants belonging to group 1 (called *stic1-1* to *stic1-5*) and two mutants belonging to group 2 (called *stic2-1* and *stic2-2*).

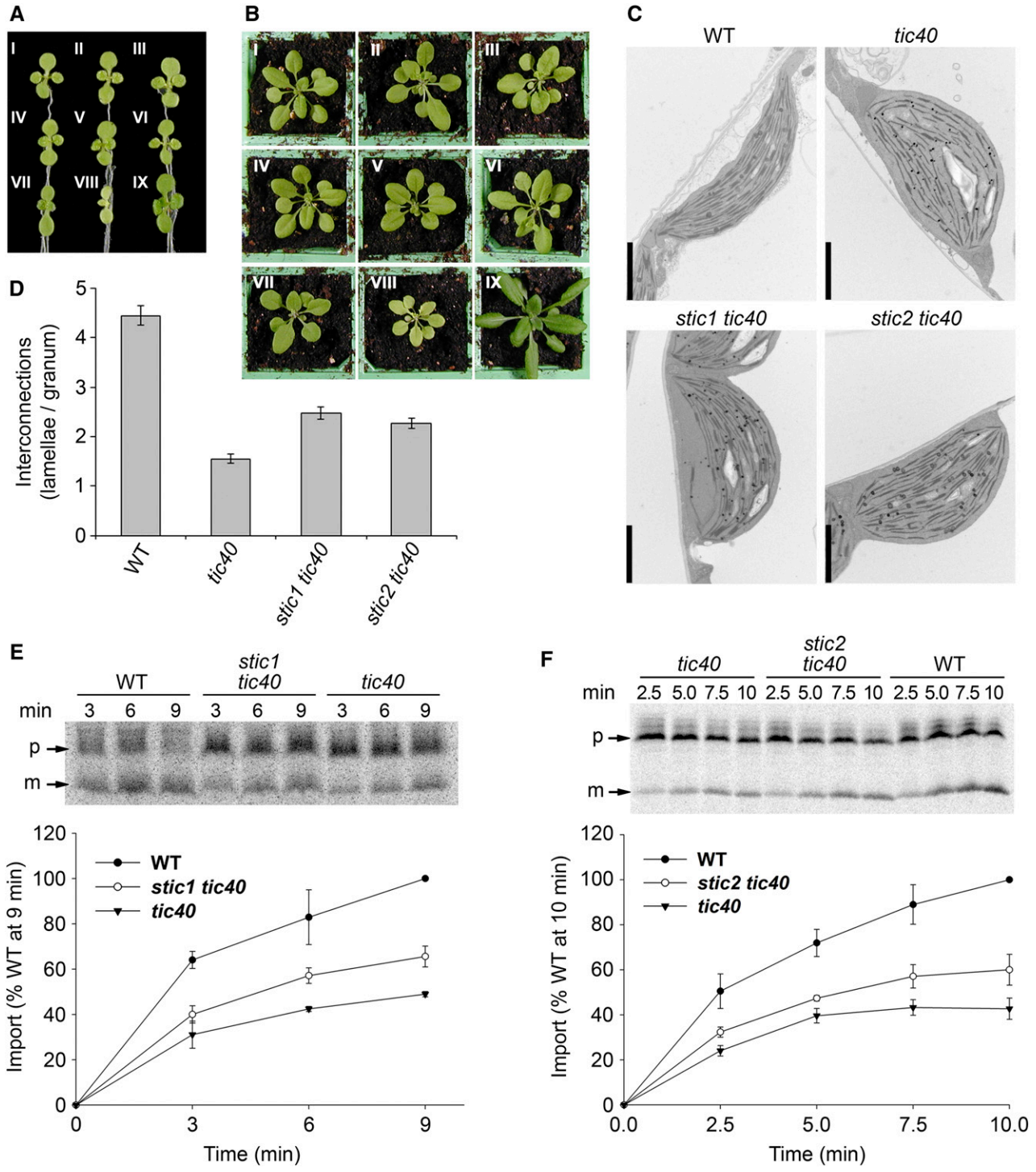

Figure 1. Suppression of the *tic40* Phenotype by the *stic* Mutations.

(A) and **(B)** Suppressor mutants selected for further characterization and mapping. Photographs showing representative 10-d-old, in vitro-grown **(A)** and 25-d-old, soil-grown **(B)** M5 generation seedlings for each selected mutant line. The plants were grown side-by-side under identical conditions alongside appropriate controls. I = 1A-1 (*stic2-1 tic40-4*), II = 1B-1 (*stic2-2 tic40-4*), III = 2A-3 (*stic1-1 tic40-4*), IV = 3A-1 (*stic1-2 tic40-4*), V = 3A-5 (*stic1-3 tic40-4*), VI = 4B-2 (*stic1-4 tic40-4*), VII = 4B-4 (*stic1-5 tic40-4*), VIII = *tic40-4*, and IX = the wild type.

The *stic* Mutations Suppress the Cellular and Organellar Structural Defects and Chloroplast Protein Import Defects of *tic40*

The *tic40* mutant phenotype is characterized by a reduced number of chloroplasts per cell and by larger chloroplasts with a swollen, more spherical morphology as well as an elevated content of plastoglobules relative to wild-type organelles (Chou et al., 2003; Kovacheva et al., 2005). Furthermore, thylakoid ultrastructure in *tic40* appears disorganized, with fewer and less stacked thylakoids (Chou et al., 2003; Kovacheva et al., 2005). To assess whether these defects were visibly reduced in the *stic* mutants, we employed light and transmission electron microscopy. Light micrographs of whole cotyledon cross sections revealed a disorganized architecture with reduced cell density in *tic40* (Supplemental Figure 2). Remarkably, as exemplified by the data shown for *stic1-1 tic40* and *stic2-1 tic40*, all of the *stic* mutants displayed a noticeable improvement in cellular architecture, with increased cell density and a more uniformly extended abaxial epidermal cell layer (Supplemental Figure 2). Transmission electron micrographs showed that the thylakoids are more developed in the *stic* mutants than in *tic40*, appearing more densely packed (Figure 1C) and having a significantly greater number of interconnections (Figure 1D). The increased cell density and improved thylakoid organization of the *stic* mutants, compared with *tic40*, most likely contribute to the larger size and greener appearance of the corresponding plants. However, the size and shape of the chloroplasts, the increased number of plastoglobules, and the number of chloroplasts per cell was not significantly different in the *stic* mutants relative to *tic40* (Figure 1C; Supplemental Figure 2).

To assess if the improvement in chloroplast development seen in the double mutants was linked to recovery of the *tic40* protein import defect described previously (Chou et al., 2003; Kovacheva et al., 2005), we performed in vitro protein import assays with chloroplasts isolated from wild-type, *tic40*, *stic1-1 tic40*, and *stic2-1 tic40* seedlings and radiolabeled Rubisco small subunit (SSU) precursor protein (Figures 1E and 1F). For both *stic1-1 tic40* and *stic2-1 tic40*, the SSU precursor was imported significantly more efficiently than for the *tic40* single mutant. The amount of mature protein detected at the final time point in each case was ~20 to 25% greater in the double mutants than in *tic40*, confirming that the suppression phenotypes are indeed linked to partial recovery of the *tic40* protein import defect.

Molecular Identification of the *stic1* and *stic2* Loci

To identify the mutations responsible for the suppression effects, the *stic* mutants were crossed to Arabidopsis plants of the Landsberg *erecta* ecotype into which the *tic40-4* mutation (originally of the Columbia-0 ecotype) had been introgressed. The F2 generations from these crosses were used initially to roughly map the mutations by assessing their linkage to polymorphic markers located on each arm of the five Arabidopsis chromosomes (Konieczny and Ausubel, 1993; Berendzen et al., 2005). This revealed that all five *stic1* mutants carry a mutation on chromosome 1, while the two *stic2* mutants mapped to chromosome 2 (Supplemental Figure 3). Further fine-mapping and sequencing, using the *stic1-4* and *stic2-1* alleles only, revealed potential splice-defect mutations in *ALB4* (G to A at nucleotide 920 relative to the ATG) for *stic1-4* (Figure 2A) and in a gene with unknown function (At2g24020; G to A at nucleotide 670 relative to the ATG) for *stic2-1* (Figure 2B). ALB4 is a paralog of the ALB3 thylakoid membrane insertase and has been proposed to cooperate with ALB3 in the insertion, assembly, or stabilization of thylakoid membrane proteins (Benz et al., 2009; Trösch et al., 2015). Both ALB4 and ALB3 are members of the conserved Alb3/Oxa1/YidC family of protein insertases (Luirink et al., 2001; Kuhn et al., 2003; Yi and Dalbey, 2005). *STIC2* is a homolog of bacterial *ybaB*, which encodes a protein implicated in membrane protein biogenesis (Skretas and Georgiou, 2010), as well as in DNA binding (Cooley et al., 2009; Jutras et al., 2012).

Further sequencing of the other *stic1* alleles confirmed the identity of the affected gene, as *stic1-1*, *stic1-3*, and *stic1-5* all had nonsense mutations in *ALB4* (nucleotide substitutions C639T, C930T, and C2102T, respectively, relative to the ATG), while *stic1-2* had a missense mutation in *ALB4* (G2213A) (Figure 2A). Similarly, the identity of the second gene was confirmed by sequencing of the *stic2-2* allele, which revealed another potential splice-defect mutation (G564A) in the At2g24020 gene (Figure

Figure 1. (continued).

(C) and **(D)** Chloroplast ultrastructure in the *stic* mutants. Transmission electron microscopy analysis of chloroplasts from cotyledons of 10-d-old, in vitro-grown seedlings of the following genotypes: wild type, *tic40-4*, and representative *stic1 tic40* (*stic1-1 tic40-4*) and *stic2 tic40* (*stic2-1 tic40-4*) double mutants.

(C) Micrographs of typical chloroplasts are shown for each genotype, which were selected on the basis of a thorough analysis of three different plants per genotype. Bars = 2 μm.

(D) To provide a quantitative measure of the extent of thylakoid development in the different genotypes, numbers of interconnecting stromal lamellae associated with each granum were counted. The presented data are from the analysis of a total of 60 grana proportionately representative of three typical chloroplasts from three different plants per genotype. Values are means and error bars correspond to the SE of the mean (n = 60).

(E) and **(F)** Analyses of chloroplast protein import efficiency in the *stic* mutants. In vitro import of radiolabeled Rubisco small subunit (SSU) precursor protein into chloroplasts isolated from 12- to 14-d-old plants of the following genotypes: wild type, *tic40*, and representative *stic1 tic40* (*stic1-1 tic40-4*) **(E)** and *stic2 tic40* (*stic2-1 tic40-4*) **(F)** double mutants. Top: Phosphor screen images of representative chloroplast protein import time-course experiments. Times shown indicate minutes (min) after the start of each import reaction. Positions of the precursor (p) and imported mature (m) forms of SSU are shown. Bottom: The amount of accumulated mature SSU protein at each time point was determined by quantifying the relevant band intensities in the top image and in two further similar experiments. Values were each expressed as a percentage of that obtained for wild-type chloroplasts at the final time point in each case. Values shown are mean percentages derived from three independent experiments; error bars show SE of the mean (n = 3).

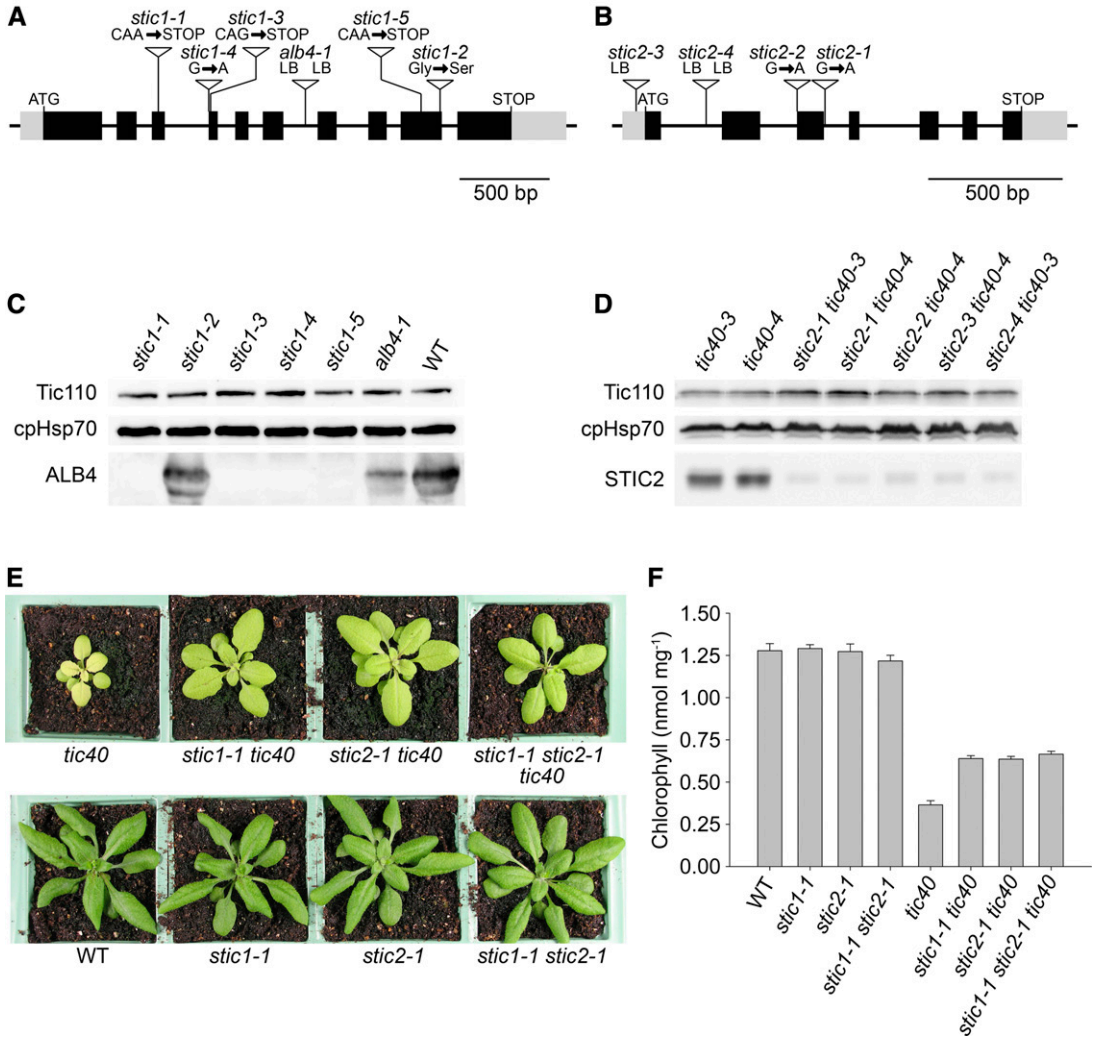

Figure 2. Molecular and Phenotypic Characterization of the *stic* Mutants.

(A) and **(B)** Schematic diagrams of *STIC1* **(A)** and *STIC2* **(B)** indicating the positions of the point mutations identified in the five *stic1* mutants (*stic1-1* to *stic1*-5) and the two *stic2* mutants (*stic2-1* and *stic2-2*). The T-DNA insertion sites for each *stic* T-DNA mutant (*alb4-1*, *stic2-3*, and *stic2-4*) as determined in this study are also indicated. Start and stop codons are shown. The gray boxes represent the 5′ and 3′ untranslated regions, whereas the black boxes and interconnecting black lines represent exons and introns, respectively.

(C) and **(D)** Analyses of STIC protein expression in the *stic* mutants. Immunoblot analyses of total seedling protein extracts (40 μg per sample) from the different *stic1* **(C)** and *stic2* **(D)** mutants. Extracts from *stic1* single mutants and wild-type control seedlings **(C)**, or from *stic2 tic40* double mutants and *tic40* control seedlings **(D)**, were analyzed. Antisera raised against Tic110, stromal Hsp70 (cpHsp70), ALB4, and STIC2 were used to detect the corresponding proteins, as indicated to the left of each blot.

(E) Visible appearance of the *stic* mutants. Photographs of representative 28-d-old plants are shown. Double and triple mutant plants in the *tic40-4* mutant background are shown next to the *tic40-4* single mutant (top), whereas single and double mutant plants in the wild-type *TIC40* background are shown next to the wild type (bottom). The plants in each set were grown side-by-side under identical conditions.

(F) Chlorophyll accumulation in the *stic* mutants. Concentrations of chlorophyll in rosette leaves of the 28-d-old mutant and control plants shown in **(E)** were quantified using a SPAD-502 meter. The values shown are means derived from measurements of six different plants and indicate nmol total chlorophyll per mg tissue fresh weight. Error bars correspond to SE of the mean (n = 6).

2B). Using RT-PCR, the predicted splicing defects of the *stic1-4*, *stic2-1*, and *stic2-2* alleles were confirmed, while the nonsense alleles *stic1-1*, *stic1-3*, and *stic1-5* were shown to have less *ALB4* transcript and the missense allele *stic1-2* to have more *ALB4* transcript relative to the wild type (Supplemental Figure 4). In addition to the obviously aberrant transcripts, all splice-defect mutants produced transcripts of similar size to the relevant wild-type transcript, albeit at reduced levels (Supplemental Figure 4). However, in the *stic1-4* mutant, these wild-type-like transcripts correspond to the loss of the first 1, 3, or 12 nucleotides of the

fourth exon. Similarly, in the case of *stic2-1* and *stic2-2*, wild-type-like transcripts carried small deletions that led to frame shifts or deletions causing the removal of a few codons and/or missense mutations. For all mutants, although the RT-PCR results suggested that they may still produce some form of the relevant STIC protein, further analysis indicated that, with the exception of *stic1-2*, this is not the case (see "Analysis of STIC Protein Expression in the *stic* Mutants" section below).

Confirmation of Suppression by Independent T-DNA Mutants and Complementation

To confirm that *STIC1/ALB4* and *STIC2* loss of function is responsible for the suppression of *tic40* in the *stic* mutants, we identified T-DNA mutants for each gene. For *STIC1/ALB4*, we obtained the *alb4-1* (SALK_136199) mutant, which was characterized previously by Gerdes et al. (2006) and shown to have a significant knockdown effect on the expression of the *ALB4* gene. We confirmed the presence and position of the T-DNA insertion (Figure 2A) as well as the knockdown effect (30.3% *ALB4* transcript relative to the wild type in 2-week-old seedlings, SE = 7.2%, $n = 6$). For *STIC2*, we identified two T-DNA mutants carrying insertions within the open reading frame of the gene: *stic2-3* (SALK_001500) and *stic2-4* (WiscDsLox 445D01) (Figure 2B). All of these *stic1* and *stic2* T-DNA mutants were crossed to *tic40*, and corresponding double homozygous mutants (*alb4-1 tic40-4*, *stic2-3 tic40-4*, and *stic2-4 tic40-3*) were identified. The phenotypes of these T-DNA double mutants were then compared with those of the original *stic1 tic40* and *stic2 tic40* double mutants and found to be visibly indistinguishable (Supplemental Figures 5A and 5C). This phenotypic similarity was also demonstrated quantitatively by measuring chlorophyll concentrations in the rosette leaves of all genotypes (Supplemental Figures 5B and 5D).

Finally, we confirmed the identity of the *STIC1* and *STIC2* genes by complementation. The *stic1-1 tic40-4* and *stic2-2 tic40-4* double mutants were transformed with constructs that drive overexpression of STIC1/ALB4 and STIC2, respectively, each with a C-terminal FLAG tag (Supplemental Figure 6). The resulting transformants were phenotypically similar to *tic40* plants (Supplemental Figures 6A and 6C) and were shown to express the respective FLAG-tagged protein (Supplemental Figures 6B and 6D). Thus, we concluded that the phenotypic reversion was caused by the expression of ALB4-FLAG and STIC2-FLAG, respectively.

Analysis of STIC Protein Expression in the *stic* Mutants

Immunoblot analyses of whole-seedling protein samples from all *stic1* mutants showed that none of the *stic1* EMS alleles, with the exception of *stic1-2*, accumulates the full-length STIC1/ALB4 protein (Figure 2C). Because the ALB4 protein expressed in the *stic1-2* mutant carries a G397S amino acid substitution due to the *stic1-2* missense mutation (Figure 2A), it is evident that this mutation impedes the function of the ALB4 C terminus and that an intact C terminus is important for ALB4 function. As reported previously, the *alb4-1* T-DNA mutant expresses the ALB4 protein at a reduced level (Gerdes et al., 2006). It is noteworthy that the antibody used to detect the ALB4 protein was raised against only the 154 most C-terminal amino acids of the protein, so the accumulation of truncated forms of the STIC1/ALB4 protein cannot be ruled out, especially as most of the mutants carry nonsense mutations (Figure 2A).

We also tested the expression of the STIC2 protein by immunoblotting (Figure 2D). Surprisingly, despite the complete lack of intact *STIC2* transcript in the *stic2-3* and *stic2-4* T-DNA mutants (Supplemental Figure 4D), we found that all *stic2* alleles accumulate small amounts of a protein that is comparable in size with STIC2 and cross-reacts with the anti-STIC2 antibody raised against the full predicted mature STIC2 protein (amino acids 49 to 182 relative to the start codon) (Figure 2D).

The Arabidopsis genome encodes a close homolog of *STIC2*, named *STIC2-Like* (*STCL*; At4g30620), with which *STIC2* shares both structural (similar exon structure; 78% amino acid sequence identity) and functional similarity (Supplemental Figure 7). A phylogenetic analysis of STIC2/STCL-related sequences from different species confirmed that this gene family is ubiquitously distributed in plants and that the two Arabidopsis genes arose from a duplication that occurred in an early ancestor of the Brassicaceae (Supplemental Figure 8 and Supplemental Data Set 1). Given the high level of similarity between the two proteins, the cross-reacting band observed in the *stic2* mutants is most likely STCL, not STIC2. Because the intensity of this band in the *stic2-1* and *stic2-2* mutants is comparable to that observed in the *stic2* T-DNA mutants (Figure 2D), we conclude that these point mutants do not accumulate significant amounts of STIC2 protein. This point was further supported by the similar analysis of plants deficient in both STIC2 and STCL (Supplemental Figure 9).

Phenotypic Characterization of the *stic1* and *stic2* Mutants

Given that the *stic1 tic40* and *stic2 tic40* mutants are visibly identical and contain similar concentrations of chlorophyll (Figures 2E and 2F), we hypothesized that the STIC proteins act in a common process (e.g., protein targeting to the thylakoids) such that the removal of one or the other protein disrupts this process. To begin to address this possibility, we generated a *stic1 stic2 tic40* triple mutant, reasoning that in an alternative scenario where *stic1* and *stic2* suppress *tic40* by disrupting different processes, their suppression effects would likely be additive. The fact that the phenotype and chlorophyll content of the triple mutant were identical to that of each double mutant, as shown in Figures 2E and 2F, supported our hypothesis that STIC1/ALB4 and STIC2 cooperate in a common process.

To determine if the *stic1* and *stic2* mutations affect chloroplast and plant development in isolation, we outcrossed the mutants to wild-type plants to obtain the single *stic1* and *stic2* mutants. As shown in Figures 2E and 2F, both single mutants look identical to, and have essentially the same chlorophyll content as, wild-type plants. This suggests that the loss of STIC proteins may be compensated for by redundancy or the operation of parallel pathways or that STIC functions become critical only under certain circumstances. The fact that the *stic1-1* mutation was not found to have a visible effect on plant development is in agreement with the findings of Gerdes et al. (2006) and Trösch et al. (2015), who characterized the *alb4-1* mutant, but in contrast to the stunted growth phenotype observed by Benz et al. (2009).

We also generated *stic1 stic2* double mutant plants by outcrossing the *stic1 stic2 tic40* triple mutant to the wild type. Like the *stic1* and *stic2* single mutants, the double mutant was phenotypically indistinguishable from wild-type plants under normal growth conditions (Figures 2E and 2F). This observation is consistent with the notion that the STIC1/ALB4 and STIC2 proteins act in a common pathway, the disruption of which is potentially compensated for by parallel processes or can be tolerated under normal conditions.

Localization of the STIC1 and STIC2 Proteins

Since the STIC2 protein is predicted to carry a transit peptide, we wished to determine if the protein is indeed targeted to chloroplasts. Thus, we generated a construct for the transient expression in protoplasts of STIC2 fused to a C-terminal YFP tag. A similar construct was made for STIC1/ALB4, although this protein was previously established as a chloroplast protein that associates with the thylakoid membranes (Gerdes et al., 2006). In addition, a free-YFP construct and a previously generated Tic110-YFP fusion construct (Bédard et al., 2007) were used as cytosol and chloroplast envelope markers, respectively. Using confocal microscopy to image transfected protoplasts, these control proteins displayed fluorescence patterns typical of cytosol and envelope localization, respectively (Figure 3A). By contrast, the ALB4-YFP signal closely overlapped with the chlorophyll autofluorescence signal, indicating that the protein likely accumulates in the thylakoids as previously reported (Gerdes et al., 2006). The STIC2-YFP protein also accumulated in the chloroplasts, confirming the TargetP (Emanuelsson et al., 2000) prediction, but the fluorescence signal in this case displayed a different profile, being concentrated in areas of the chloroplasts where the chlorophyll fluorescence signal was least intense, which suggests that the protein accumulates in the stroma (Figure 3A). A similar STCL-YFP fusion displayed the same localization profile (Supplemental Figure 7D).

To confirm the localizations of the STIC proteins using an alternative approach, chloroplasts were isolated from seedlings expressing the ALB4-FLAG and STIC2-FLAG fusion proteins described earlier and then subfractionated by sucrose density-gradient centrifugation to obtain stromal, envelope, and thylakoidal fractions. Immunoblotting analysis of the different fractions using antibodies against the FLAG tag and the following control proteins enabled us to assess the localization of the STIC proteins biochemically; the controls were Tic110 (envelope), LHCP (thylakoid), ALB3 (thylakoid), and the small subunit of Rubisco (SSU; stroma). In accordance with the microscopy data, the ALB4-FLAG protein was found exclusively in the thylakoid fraction (Figure 3B), while the STIC2-FLAG protein was detected exclusively in the stromal fraction (Figure 3C). The control proteins largely behaved as expected, although we did detect some Tic110 in the thylakoid fractions, indicating that these were somewhat contaminated with envelopes (Figures 3B and 3C), as is often the case in such subfractionation experiments.

To assess the possibility that the localization of STIC1/ALB4 is dynamic, enabling colocalization with Tic40 in the envelope at specific developmental stages, we similarly analyzed chloroplasts isolated from plants of different ages, including some that were of approximately the same age as those used for the microscopy (5 weeks old; Supplemental Figure 10). In each case, we failed to detect any ALB4-FLAG protein in the envelope fraction, indicating that the protein is stably confined to the thylakoid membrane.

The accumulation of STIC2 in the stroma is not surprising because the protein does not possess any hydrophobic regions that might form a transmembrane helix to anchor it in a membrane (Krogh et al., 2001). However, a previously reported chloroplast proteome study suggested that some STIC2 protein is associated with the thylakoids (Peltier et al., 2004), presumably as a peripheral protein via protein-protein interactions. The fact that no STIC2-FLAG protein was detected in the thylakoids in our study suggests that either the chloroplast thylakoid fraction analyzed by Peltier et al. (2004) was slightly contaminated with stromal proteins, or the amount of STIC2-FLAG that associates with the thylakoids is so low as to be beyond the limits of detection in our assay.

Chloroplast Morphology and Ultrastructure of the *stic* Mutants

Because STIC1/ALB4 and STIC2 are both chloroplast proteins, we sought to gain further insight into their functions by characterizing chloroplast ultrastructure in corresponding single mutant plants, which at a macroscopic level are indistinguishable from the wild type. As shown in Figure 4A (upper micrographs), we observed that the cotyledon chloroplasts of *stic1* and *stic2* seedlings have an unusual morphology: In both cases, the chloroplasts appeared swollen and less appressed to the cell periphery than wild-type chloroplasts. The shape difference was quantified by measuring the length and width of chloroplast cross sections and comparing the length/width ratio with that of the wild type (Figure 4B). In both mutants, this ratio is roughly three-quarters that of wild-type chloroplasts, confirming that they are more spherical.

Upon observation at higher magnification, the thylakoid membrane networks in the *stic* mutants appeared to be as developed and complex as those of wild-type chloroplasts (Figure 4A, lower micrographs): Comparable grana of variable thickness were seen in all genotypes, interconnected by networks of stromal lamella membranes, dispersed throughout each chloroplast cross section. Nonetheless, the lamellae were found to be less parallel and tightly packed (i.e., more loosely distributed) in the mutants, possibly due to the rounder shape of the chloroplasts. Interestingly, a significantly higher number of plastoglobules (lipid bodies) were visible in the mutant chloroplasts, as illustrated in Figure 4C, pointing toward a thylakoid biogenesis defect (Rudella et al., 2006).

In relation to *stic1*, these observations are consistent with those made by Gerdes et al. (2006) and Trösch et al. (2015) using the *alb4-1* T-DNA insertion mutant. The appearance of the *stic* mutant chloroplasts is reminiscent of the previously described swollen chloroplast phenotype of *tic40* plants (Kovacheva et al., 2005; Bédard et al., 2007), although in that case the thylakoid membrane system was much less developed. The chloroplast morphology defect is possibly more similar to that observed in the *vipp1* knockdown mutant (Zhang et al., 2012), which is believed to have an inner envelope membrane integrity defect.

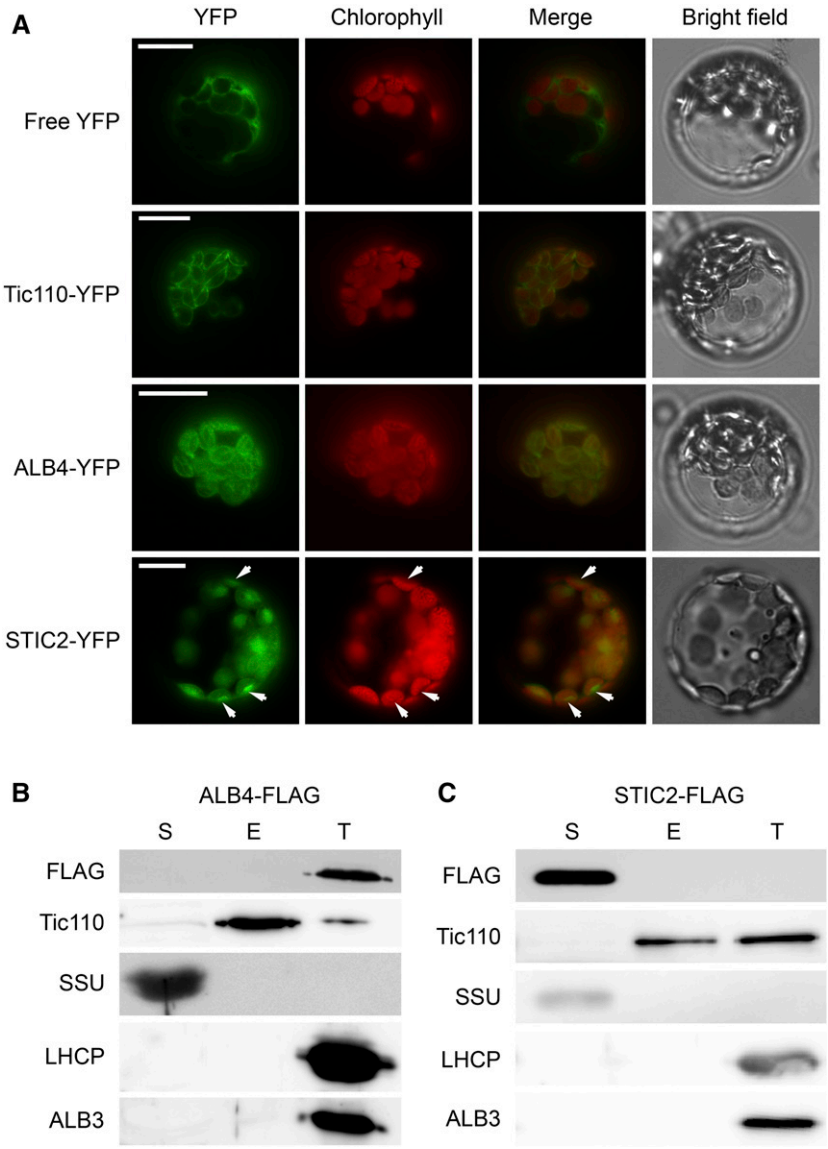

Figure 3. Localization of the STIC1/ALB4 and STIC2 Proteins.

(A) Confocal microscopy analysis. Arabidopsis protoplasts transiently expressing the following proteins were analyzed by confocal microscopy: YFP (Free YFP), Tic110-YFP, STIC1/ALB4-YFP, and STIC2-YFP; all of the YFP fusion proteins carried a C-terminal YFP tag. Representative protoplasts are shown. In each case, YFP fluorescence, chlorophyll autofluorescence, merged YFP and chlorophyll fluorescence, and bright-field images are shown. White arrowheads in the STIC2-YFP micrographs indicate areas of the chloroplasts where the YFP signal is clearly accumulated but a strong chlorophyll signal is lacking. Bars = 12.68 μm.

(B) and **(C)** Chloroplast subfractionation analysis. Chloroplasts isolated from transgenic seedlings overexpressing C-terminally FLAG-tagged STIC1/ALB4 **(B)** or STIC2 **(C)** were separated into stroma (S), envelope (E), and thylakoid (T) enriched fractions prior to immunoblotting (~15 μg of each sample was analyzed). An anti-FLAG antibody was used to detect the STIC1/ALB4-FLAG and STIC2-FLAG proteins, while antisera raised against Tic110, SSU, LHCP, and ALB3 were used to detect the corresponding reference proteins.

Specificity of the Suppression Effects of *stic1* and *stic2*

To determine if the suppression effects of the *stic* mutations are specific to *tic40*, or more general, we crossed the single *stic1-1* or *stic2-1* mutants to several other protein import mutants: *ppi1*, *toc75-III-3*, *hsp93-V*, and *tic110*. All of these mutants display a degree of chlorosis linked to defective import, with the lesions occurring at either the outer membrane (*ppi1* is a null mutant for the Toc33 receptor; *toc75-III-3* is a point mutant of the Toc75 channel) or the inner membrane (*hsp93-V* is a null mutant for the Hsp93/ClpC chaperone; *tic110* is a heterozygous mutant for a chaperone recruitment scaffold protein) (Jarvis et al., 1998; Kubis et al., 2003; Kovacheva et al., 2005; Stanga et al., 2009; Huang et al., 2011). Double mutants were generated and their phenotypes were

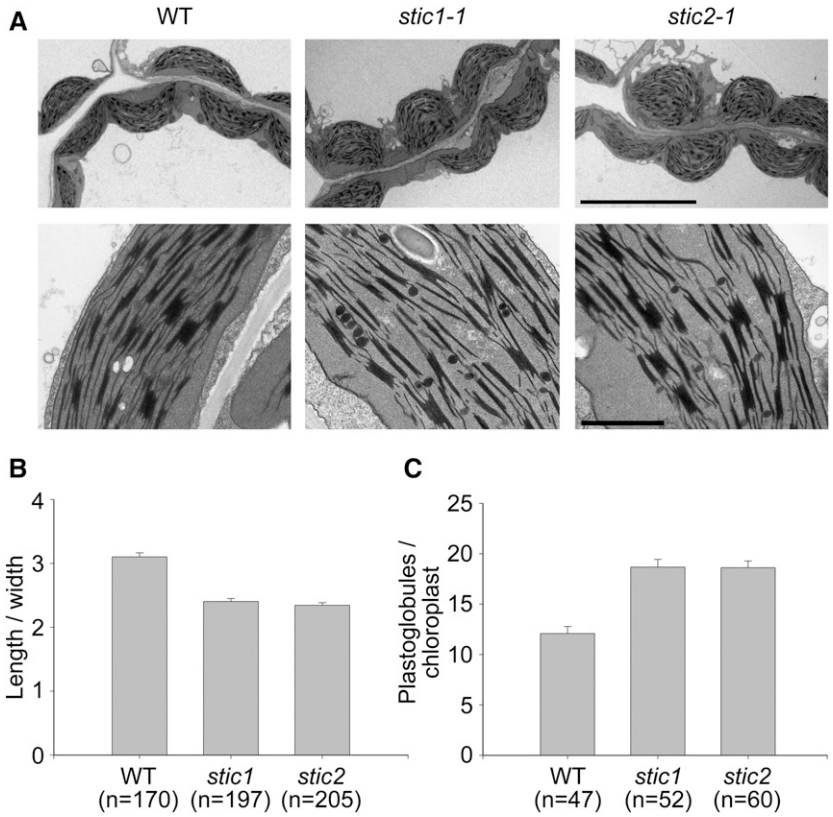

Figure 4. Morphology and Ultrastructure of *stic1* and *stic2* Mutant Chloroplasts.

(A) Transmission electron micrographs of chloroplasts in cotyledons of 10-d-old, in vitro-grown seedlings of the following genotypes: wild type and representative single *stic* mutants, *stic1-1* and *stic2-1*. Whole-organelle (top) and thylakoid close-up (bottom) images are shown for each genotype. Bars = 10 and 1.5 μm, respectively. Typical micrographs are shown, which were selected on the basis of a thorough analysis of three different plants per genotype.
(B) Analysis of chloroplast shape. Using the electron micrographs described in **(A)**, chloroplast length and width measurements for a total of *n* different organelle cross sections were made (values of *n* are shown in the figure). Roughly equal numbers of chloroplasts from two different seedlings per genotype were analyzed. The length and width values were used to derive ratios, as an indicator of chloroplast shape, and the average ratio (±SE) for each genotype is shown.
(C) Analysis of plastoglobule numbers. Using the electron micrographs described in **(A)**, the number of plastoglobules per chloroplast cross section in a total of *n* different organelles was counted (values of *n* are shown in the figure). Roughly equal numbers of chloroplasts from three different seedlings per genotype were analyzed. The average number (±SE) for each genotype is shown.

compared with those of the corresponding single import mutants (Supplemental Figure 11). Most of the double mutants analyzed were double homozygotes, but because the *tic110* mutation is embryo lethal in the homozygous state and causes chlorosis in the heterozygous state (Inaba et al., 2005; Kovacheva et al., 2005), the corresponding double mutants were heterozygous for *tic110*.

As exemplified for the import mutants in combination with *stic1-1* (Supplemental Figure 11A), the double mutants appeared in all cases identical to the corresponding single mutants, regardless of the severity of the chlorotic phenotype displayed. To quantitatively assess these observations, chlorophyll concentrations in each pair of single and double mutants were measured and used to calculate average ratios (Supplemental Figure 11B). In all cases, the ratios obtained were approximately equal to 1, indicating no difference between the double and single mutants. A similar result was obtained for the import mutants in combination with *stic2-1* (Supplemental Figure 11C). These results contrast markedly with those obtained for the *stic tic40* double mutants, where the equivalent chlorophyll content ratio values obtained were ~1.8 to 1.9. Thus, the results clearly indicate that the *stic* mutations are not general suppressors of import deficiency. We conclude that the suppression effects mediated by *stic1* and *stic2* are quite specific for *tic40*, implying a close functional connection between the STIC proteins and Tic40.

Genetic Interactions between the *stic* Mutations and Thylakoid Protein Targeting Mutations

Given the similarity between STIC1/ALB4 and ALB3 and the well-established role of the latter in thylakoid protein biogenesis, and the genetic evidence pointing toward roles for the STIC proteins in a common process (Figures 2E and 2F), we wished to investigate if the STIC proteins act in thylakoid protein transport. To begin to address this possibility, further genetic interaction tests were performed, this time with mutants for components of the different thylakoid targeting pathways; i.e., the cpSec, cpTat, and cpSRP

pathways. The mutants used in this analysis were as follows: *cpsecA1* (null for the cpSecA1 ATPase), *hcf106* (null for the chloroplast TatB homolog), *cpsrp54-3*, *cpsrp43-2*, and *cpftsY-1* or *cpftsY-2* (null for the cpSRP54, cpSRP43, and cpFtsY components, respectively, of the cpSRP pathway; Supplemental Figure 12A). Again, we generated double mutants with *stic1* and *stic2* and compared them to the corresponding single thylakoid targeting mutants (Figure 5; Supplemental Figures 12B to 12D).

The *cpsecA1* and *hcf106* mutants have seedling-lethal, albino phenotypes similar to that of the *alb3* mutant of the cpSRP pathway, and so cannot survive when grown on soil but can be maintained in vitro on medium containing sucrose (Liu et al., 2010). It was recently shown that the *alb4-1* mutation interacts synergistically with the *alb3-1* null mutation, producing seedlings that are even more chlorotic and weak than the single *alb3* mutant (Trösch et al., 2015). This was interpreted to indicate that there is a degree of functional redundancy between the two affected proteins and that ALB4 participates in the cpSRP pathway or in a parallel pathway that performs a similar role. In marked contrast, no synergistic effects were observed when *stic1* and *stic2* were combined with the *cpsecA-1* and *hcf106* mutations, as the double mutants were phenotypically indistinguishable from the corresponding albino single mutants (Figures 5A and 5B). If we assume that the cpSec and cpTat pathways are not completely blocked in these mutants, respectively, then the failure of the *stic* mutations to accentuate the *secA1* and *hcf106* phenotypes suggests that the STIC proteins do not participate in these pathways.

The *cpsrp54*, *cpsrp43*, and *cpftsY* mutants are all chlorotic, but they are viable and phenotypically less severe than the albino mutant *alb3*: The *cpsrp54* and *cpsrp43* mutants produce rosette leaves that are initially yellow but then become progressively greener (Figures 5C and 5D; Supplemental Figures 12B to 12D) (Amin et al., 1999; Klimyuk et al., 1999; Yu et al., 2012), whereas *cpftsY* is more severely chlorotic, remains yellow throughout development, and displays stunted growth (Figures 5E and 5F) (Asakura et al., 2008). As shown in Figures 5C to 5F, the *stic cpsrp54* and *stic cpftsY* double mutants were all significantly smaller and more chlorotic than the corresponding single mutants, indicating that both *stic* mutations interact synergistically with *cpsrp54* and *cpftsY*. By contrast, similar synergistic interactions were not detected in the *stic1 cpsrp43* and *stic2 cpsrp43* double mutants (Supplemental Figures 12B to 12D), implying that the STIC proteins do not act in the canonical cpSRP43 pathway for LHCP targeting.

Overall, these genetic data strongly support the notion that the STIC proteins act together in a specialized cpSRP pathway that is distinct from the cpSec and cpTat pathways. This conclusion is consistent with the thylakoid morphological defects (Figure 4A) and the accumulation of plastoglobules (Figure 4C) seen in the *stic* mutants, and with the genetic evidence suggesting that the two proteins act in a common process (Figures 2E and 2F).

STIC2 Interacts with the C Termini of ALB4 and ALB3 in Vitro

We wished to investigate whether the STIC proteins can interact physically with each other. To address this possibility, we employed in vitro pull-down experiments using recombinant proteins expressed in bacteria (Figures 6A to 6C). For this work, we used an N-terminally tagged form of the STIC1/ALB4 C terminus (His-ALB4C; residues 345 to 498 of the preprotein), representing most of the stromal C-terminal domain (Falk et al., 2010), and an N-terminally tagged form of the mature STIC2 protein (GST-STIC2; residues 49 to 182 of the preprotein) (Figure 6A, left side). Equal amounts of soluble lysate from bacteria expressing each protein were mixed together, and then the His-ALB4C protein was affinity purified. The GST-STIC2 protein copurified efficiently with His-ALB4C in the absence of significant amounts of any other protein, providing strong evidence for a direct interaction between STIC2 and the C terminus of STIC1/ALB4 (Figure 6A, left side). By contrast, when His-ALB4C was replaced in the assay by the His-tagged LTD stromal targeting factor (Ouyang et al., 2011), significant GST-STIC2 copurification was not detected (Figure 6B). This demonstrated that GST-STIC2 does not associate nonspecifically with the affinity resin used to purify the His-tagged proteins, confirming that the detected copurification (Figure 6A) reflects a genuine protein-protein interaction.

The *stic1-2* mutant carries a glycine-to-serine missense mutation (G397S) that affects the stromal domain of STIC1/ALB4 employed in the in vitro pull-down experiments. In view of the evidence indicating that STIC1/ALB4 and STIC2 act in a common pathway (Figure 2), we reasoned that a consequence of this mutation might be to perturb the interaction between the STIC proteins. To address this possibility, we introduced the G397S mutation into the pull-down construct (His-ALB4C-G397S) and used it in further pull-down studies with the GST-STIC2 protein (Figure 6A, right side). Although identical amounts of His-ALB4C-G397S and His-ALB4C were employed, in simultaneous experiments conducted in parallel, substantially reduced binding of GST-STIC2 was observed with His-ALB4C-G397S relative to wild-type His-ALB4C (on average, 17% over the four elutions, SE = 4%). These data support the notion that STIC2 interacts specifically with the C terminus of STIC1/ALB4 and indicate that the Gly-397 residue is important for this interaction.

The functional differences between the ALB3 and ALB4 proteins are believed to be mainly attributable to their different stromal C termini. While ALB3 contains two conserved motifs (Motifs II and IV) important for association with the LHCP targeting factor cpSRP43, ALB4 lacks these domains (Falk et al., 2010). Gly-397 of ALB4 has been proposed to be part of Motif III that is present in both ALB4 (residues 397 to 414) and ALB3 (residues 386 to 403) (Falk et al., 2010). Thus, it is possible that this motif is also important for STIC2 interaction with ALB3. Therefore, to determine if the C terminus of ALB3 can also directly interact with GST-STIC2, we conducted further pull-down studies using an N-terminally tagged form of the ALB3 C terminus (His-ALB3C; residues 361 to 462 of the preprotein). As shown in Figure 6C, His-ALB3C also efficiently pulled down the GST-STIC2 protein, indicating that STIC2 interacts not only with STIC1/ALB4 but also with ALB3, further supporting the notion that STIC2 plays a role in protein targeting to the thylakoids.

BiFC Analysis of the Interaction between ALB3, ALB4, and STIC2

To provide in vivo corroboration of the interactions observed in vitro (Figures 6A to 6C), we employed bimolecular fluorescence

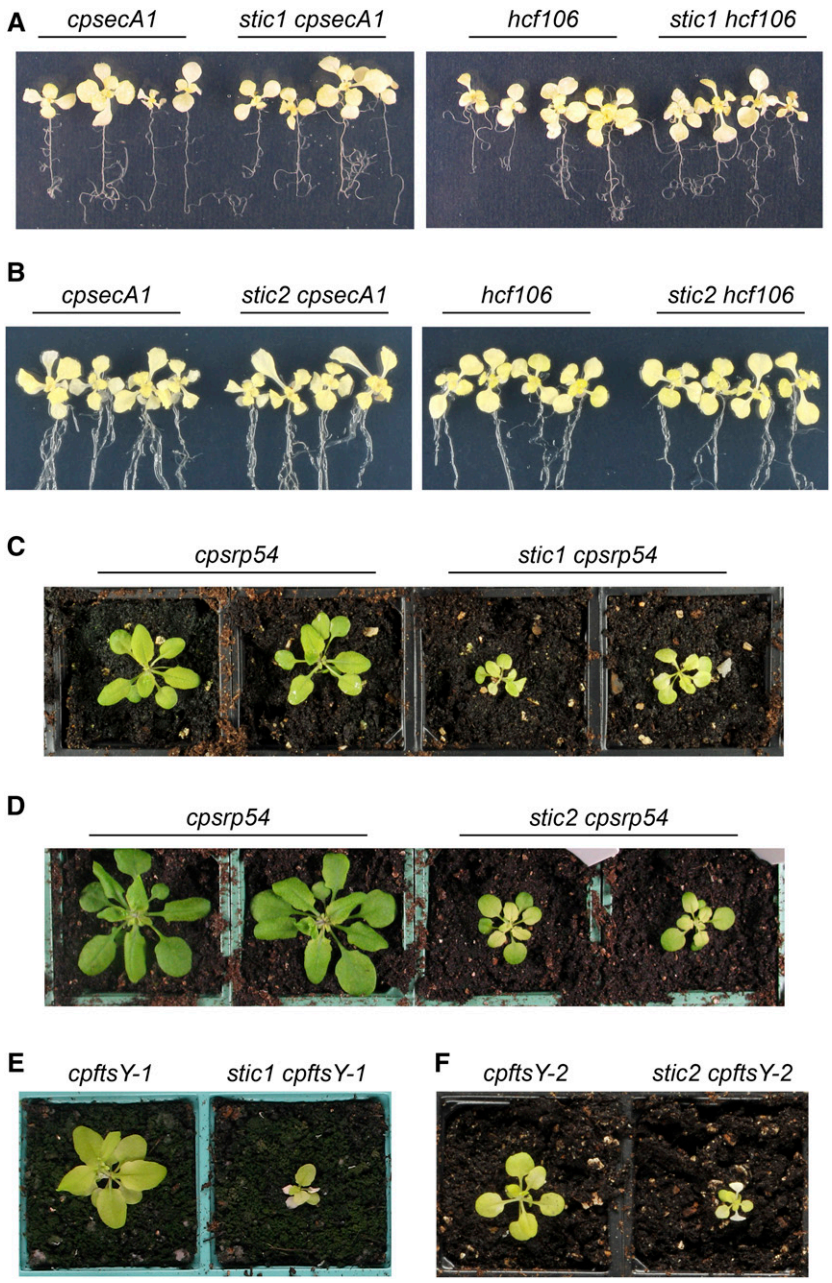

Figure 5. Specific Genetic Interactions between *stic* Mutations and cpSRP Pathway Mutations.

Double mutant plants carrying one or the other *stic* mutation together with a mutation affecting one of three well-characterized thylakoid protein targeting pathways were generated and then compared phenotypically with single mutant control plants. The thylakoid targeting mutants analyzed were as follows: *cpsecA1* (**[A]** and **[B]**; affecting the cpSec pathway), *hcf106* (**[A]** and **[B]**; affecting the cpTat pathway), *cpsrp54-3* (**[C]** and **[D]**), and *cpftsY-1* or *cpftsY-2* (**[E]** and **[F]**, respectively) (all affecting the cpSRP pathway). The *stic* mutant alleles employed in this analysis were as follows: *stic1-1* (**[A]**, **[C]**, and **[E]**), *stic2-1* **(B)**, *stic2-3* **(D)**, and *stic2-4* **(F)**. All plants were initially grown in vitro under standard conditions before being transplanted after 8 to 12 d growth, either to MS medium supplemented with 3% (w/v) sucrose (**[A]** and **[B]**) or soil (**[C]** to **[F]**). The plants were analyzed after a total of 3 to 4 weeks of growth.

complementation (BiFC) in transfected Arabidopsis protoplasts (Lee et al., 2008). Thus, the STIC coding sequences were inserted into vectors that generate fusions to the N-terminal or C-terminal parts of yellow fluorescent protein (nYFP and cYFP, respectively). Various nYFP and cYFP fusion vector pairs were then cotransfected and imaged by confocal microscopy. In this system, YFP fluorescence is only observed when the nYFP and cYFP parts are brought into close proximity by the interaction of the fused proteins (in this case, the STIC1/ALB4, STIC2, and ALB3 proteins), enabling reconstitution of a complete, functional YFP protein

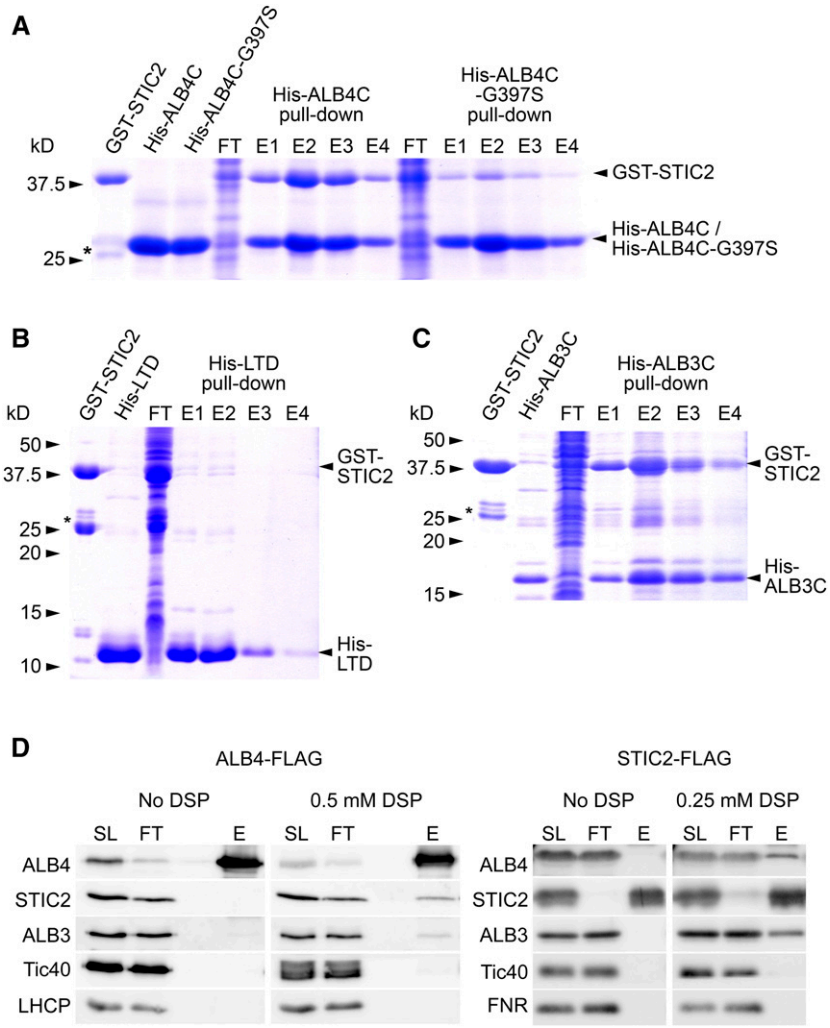

Figure 6. Physical Interactions between STIC2 and the STIC1/ALB4 and ALB3 Proteins.

(A) to **(C)** In vitro pull-down analysis. Experiments were performed using lysates of *E. coli* cells expressing recombinant GST-STIC2 (**[A]** to **[C]**), His-ALB4C **(A)**, His-ALB4C-G397S **(A)**, His-LTD **(B)**, and/or His-ALB3C **(C)**. In each experiment, equal amounts of lysate containing GST-STIC2 and one of the His-tagged proteins were incubated together, and then the His-tagged protein was purified using Ni-NTA resin prior to analysis by SDS-PAGE. In each gel, individually purified protein samples from the relevant lysates were included as reference controls (left side, with angled labels); the asterisks indicate a truncated form of the GST-STIC2 protein that appeared in the lysates to a variable degree. The flow-through (FT) samples contained proteins not bound by the Ni-NTA resin, whereas the imidazole elution fractions (E1–E4) contained proteins that were bound by the resin. All of the gels were stained with Coomassie blue. For all samples, 10 μL was loaded per lane.

(D) Co-IP analysis. Experiments were performed with chloroplasts isolated from 12- to 14-d-old, in vitro-grown wild-type plants overexpressing either STIC1/ALB4-FLAG (left side) or STIC2-FLAG (right side). Chloroplasts were solubilized with DDM directly after isolation (left side in each case) or after treatment with 0.25 to 0.50 mM of the membrane-permeable cross-linker DSP (right side in each case) and subjected to anti-FLAG immunoprecipitation. All samples were analyzed by immunoblotting. Amounts equivalent to ~25 μg of protein for solubilized chloroplast lysate (SL) and for the co-IP flow-through (FT) were loaded, whereas one-third or one-sixth of elution (E) samples was loaded for the STIC1/ALB4-FLAG and STIC2-FLAG samples, respectively. Antisera raised against STIC1/ALB4, STIC2, ALB3, Tic40, and LHCP or FNR were used to detect the corresponding proteins.

(Lee et al., 2008). As a positive control for transfection, the ALB4-YFP plasmid was used on its own (Figure 7); this control produces a stronger signal than BiFC because it does not depend on the interaction of two proteins.

Protoplasts that were transfected with both STIC2-nYFP and ALB4-cYFP constructs produced a clear fluorescence signal that overlapped with the chlorophyll signal, as observed in the positive control (Figure 7). Neighboring untransfected protoplasts or protoplasts transfected with only one of the plasmids did not produce a fluorescence signal, although chlorophyll fluorescence was observed (Supplemental Figure 13). In the reciprocal experiment, protoplasts doubly transfected with STIC2-cYFP and ALB4-nYFP produced an identical signal. When ALB4 was replaced with the mutated form (G397S), fluorescence signals were

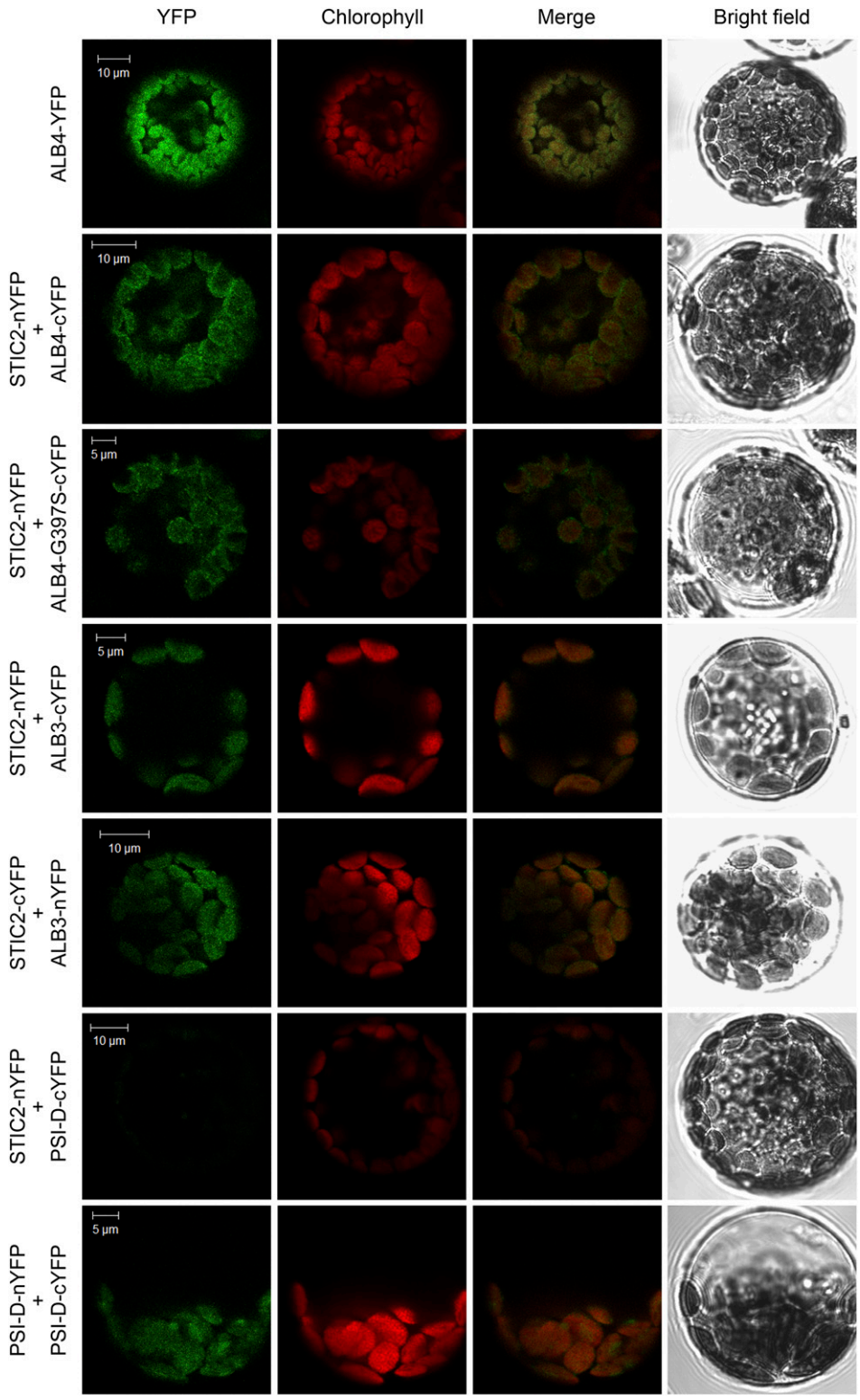

Figure 7. In Vivo Analysis of Interactions between STIC2 and the STIC1/ALB4 and ALB3 Proteins.

BiFC analysis of protein-protein interactions was performed by studying Arabidopsis protoplasts coexpressing proteins fused to complementary N-terminal (nYFP) and C-terminal (cYFP) fragments of the YFP protein. The images shown are representative confocal micrographs of protoplasts expressing STIC1/ALB4 with a complete YFP tag (ALB4-YFP; this served as a positive control) or the following fusion protein pairs: STIC2-nYFP with ALB4-cYFP,

also observed (Figure 7); detection of this interaction may reflect the ability of mutant ALB4 to residually bind STIC2 (Figure 6B) and be aided by the overexpression of both interaction partners. Alternatively, if ALB4-G397S-cYFP homooligomerizes with endogenous ALB4 or heterooligomerizes with ALB3, interaction of STIC2-nYFP with the endogenous proteins may be sufficient to result in fluorescence due to close proximity of the YFP moieties. Clear fluorescence signals were also observed for both STIC2-ALB3 combinations (STIC2-nYFP with ALB3-cYFP; STIC2-cYFP with ALB3-nYFP; Figure 7), while no signals were observed in the negative control, STIC2-nYFP with PSI-D-cYFP (Figure 7). The PSI-D-cYFP fusion is a valid negative control here, as it was shown to be expressed and able to interact with PSI-D-nYFP in chloroplasts (Figure 7; Supplemental Figure 13) (Xia et al., 1998; Kudla and Bock, 2016).

Overall, our BiFC data confirm the data obtained from the in vitro pull-down assays and provide clear in vivo support for the interaction of STIC2 with both ALB4 and ALB3.

STIC2 Can Be Cross-Linked to Both ALB4 and ALB3 in Coimmunoprecipitation Experiments

To further corroborate the positive interaction results from the in vitro pull-down and in vivo BiFC studies, a complementary approach was used: Anti-FLAG coimmunoprecipitation (co-IP) from chloroplasts isolated from wild-type plants that overexpress ALB4-FLAG or STIC2-FLAG proteins (Figure 6D). Using freshly isolated chloroplasts solubilized with the nonionic detergent dodecyl maltoside (Figure 6D, left side of each panel), the ALB4-FLAG and STIC2-FLAG proteins were efficiently immunoprecipitated, eluted from the anti-FLAG resin with SDS buffer, and detected with ALB4 and STIC2 antisera, respectively. However, no significant interaction between the STIC proteins was detectable, nor was there any significant interaction between the STIC proteins and ALB3 or Tic40. The photosynthetic proteins LHCP and ferredoxin-NADP reductase (FNR) used as controls in these assays were also absent from the eluates.

Our failure to detect interactions in our initial studies prompted us to repeat the experiments following treatment with the membrane-permeable chemical cross-linker dithiobis succinimidyl propionate (DSP), which can facilitate the detection of transient or weak interactions that might otherwise be lost during the purification procedures (Figure 6D, right side of each panel). In these experiments, the control proteins LHCP and FNR were again absent from the eluted fractions, providing a clear indication of specificity. No interactions between the STIC proteins and Tic40 were detected, but on this occasion, the ALB3 protein was coimmunoprecipitated with STIC2-FLAG and with ALB4-FLAG in accordance with the results of Trösch et al. (2015) (Figure 6D). Moreover, the STIC2 protein copurified with STIC1-FLAG, and the STIC1/ALB4 protein copurified with STIC2-FLAG, in the reciprocal experiments, confirming that the two STIC proteins can indeed interact physically with each other.

DISCUSSION

Our screen for suppressors of the *tic40* mutant identified two loci, corresponding to the *STIC1/ALB4* gene and the previously uncharacterized *STIC2* gene. Genetic analyses implied that STIC1/ALB4 and STIC2 cooperate in a common pathway (Figure 2), a notion that was supported by the fact that the proteins interact physically with each other (Figures 6 and 7). Thus, we concluded that the two proteins act together in thylakoid membrane biogenesis, as elaborated below.

STIC1/ALB4 Is a Member of a Conserved Family of Membrane Protein Biogenesis Factors

ALB4 was discovered as a paralog of ALB3 in Arabidopsis, with both proteins belonging to the Alb3/Oxa1/YidC family of membrane insertases (Gerdes et al., 2006). Mutants of ALB3 are particularly affected in the accumulation of the light-harvesting system and display a strongly chlorotic/albino phenotype (Sundberg et al., 1997; Bellafiore et al., 2002; Asakura et al., 2008). By contrast, *alb4* mutant plants show no macroscopic defects, although the thylakoids in such mutants are structurally aberrant (Figures 2 and 4) (Gerdes et al., 2006). In addition to its role in the insertion of imported LHCPs, ALB3 is also thought to participate in the targeting of cotranslationally inserted proteins (e.g., D1), interacting with ribosome nascent chains together with VIPP1 and cpSecY (Pasch et al., 2005; Walter et al., 2015). Thus, it is likely that ALB4 plays a specialized role in the insertion and/or assembly of a subset of proteins (Trösch et al., 2015).

The phenotypic differences between *alb3* and *alb4* mutants may reflect expression level differences between ALB3 and ALB4, functional differences between ALB3 and ALB4, and/or the operation of parallel pathways (Trösch et al., 2015). It has been suggested that ALB4 stabilizes assembly intermediates of the ATP synthase complex (Benz et al., 2009) and that it participates in the insertion or assembly of cytochrome b_6f complex components (Trösch et al., 2015). Thus, ALB4 may have a chaperone-like function, assisting the folding and assembly of transmembrane proteins into complexes, which is another role generally attributed to the Alb3/Oxa1/YidC protein family (Wang and Dalbey, 2011).

STIC2 Is Homologous to the Bacterial Protein YbaB

The STIC2 protein and its homolog STCL were previously uncharacterized, but they share homology with the bacterial protein YbaB (Supplemental Figures 7 and 8). Although YbaB itself

Figure 7. (continued).

ALB4-G397S-cYFP, ALB3-cYFP, or PSI-D-cYFP (the latter served as a negative control); STIC2-cYFP with ALB3-nYFP; and PSI-D-nYFP with PSI-D-cYFP (which demonstrated that the negative control protein PSI-D-cYFP can be expressed and is competent to reconstitute YFP when associated with an appropriate interaction partner). For each protoplast, YFP fluorescence, chlorophyll autofluorescence, merged YFP and chlorophyll fluorescence, and bright-field images are shown. Bars representing 5 or 10 μm are shown for each set of images.

is far from well characterized, it has been implicated in membrane biogenesis (Skretas and Georgiou, 2010): Coexpression of the native *ybaB* gene enhanced the accumulation of membrane-integrated heterologous proteins up to 10-fold in *Escherichia coli*. Although DNA binding activity has also been suggested for YbaB (Cooley et al., 2009; Jutras et al., 2012), the overall negative charge of STIC2 (charge at pH 7.0, –3.93; pI 4.95) and STCL (charge at pH 7.0, –1.94; pI 5.40) make this property seem unlikely. The crystal structure of YbaB shows a tweezer-like dimer formation (Lim et al., 2003), which based on homology modeling analysis is likely to be shared by STIC2 and STCL (Supplemental Figure 14) (Kelley et al., 2015).

STIC Proteins Cooperate in a Common, cpSRP-Related Thylakoid Protein Targeting Pathway

Because STIC1/ALB4 has already been assigned a function in thylakoid protein biogenesis (Trösch et al., 2015), it is likely that STIC2 participates in the same process. This notion was further supported by our phenotypic analysis of the single *stic* mutants. Although the *stic* mutants were visibly indistinguishable from the wild type, they had swollen chloroplasts with disordered (less parallel) thylakoids and an accumulation of plastoglobules (Figures 2 and 4). These phenotypes are consistent with those of the *alb4-1* knockdown mutant described previously (Gerdes et al., 2006), and overall they support our hypothesis that STIC1/ALB4 and STIC2 cooperate in thylakoid membrane biogenesis.

Our data showed that STIC2 is a stromal protein lacking detectable association with the thylakoid membranes (Figure 3). With STIC1/ALB4 being an integral thylakoid membrane protein, this makes a stable interaction between STIC1/ALB4 and STIC2 seem implausible. Indeed, the addition of a cross-linker was required to detect coimmunoprecipitation of the two proteins (Figure 6), suggesting that the interaction is not structural but functional and of a transient nature. STIC2 potentially acts upstream of STIC1/ALB4 as a stromal sorting factor that delivers targets to the membrane. The STIC1/ALB4 C terminus can bind STIC2 in vitro, and Gly-397 of mature STIC1/ALB4 is important for this interaction in vitro (Figure 6). In fact, Gly-397 may be essential for ALB4 function because *stic1-2* (which carries the G397S substitution) has an identical *tic40* suppression phenotype to nonsense mutants such as *stic1-5* (Figures 1 and 2; Supplemental Figure 5). It is also pertinent that both ALB4 and STIC2 can interact with ALB3 in vitro and in vivo (Trösch et al., 2015) (Figures 6 and 7). Given that direct STIC2-ALB3 and STIC2-ALB4 interactions were both detected, one may speculate that STIC2 mediates the interaction between ALB3 and ALB4.

The interactions with ALB3 suggested a functional link between the STIC proteins and the cpSRP pathway. In support of this notion, the phenotypes of the *cpsrp54* and *cpftsy* mutants became much more severe when combined with either *stic1* or *stic2* (Figure 5). No such effects were observed when *stic1* and *stic2* were crossed to mutants affected in protein import (Supplemental Figure 11) or the cpSec and cpTat pathways (Figure 5), indicating that the observed synergistic effects are highly specific for the cpSRP pathway. However, the lack of physical interaction between STIC2 and LTD (Figure 6), and the absence of synergistic genetic interaction between the *stic* mutants and a null cpSRP43 mutant (Supplemental Figure 12), indicates that STIC2 and ALB4 do not participate in the main transport pathway for delivering LHCP proteins. Thus, STIC1/ALB4 and STIC2 may cooperate in thylakoid membrane biogenesis as part of a cpSRP43-independent cpSRP pathway for a specific subset of clients or a putative alternative LHCP transport pathway (Tzvetkova-Chevolleau et al., 2007). Interestingly, *STIC2* has a similar expression profile to some nucleus-encoded chloroplast ribosomal protein genes (e.g., *PSRP4* and *PRPL35*) (Aoki et al., 2016), suggesting another possible role in the cotranslational targeting via ALB4 or ALB3. Accordingly, cpSRP54 and cpFtsY are both implicated in cotranslational insertion via ALB3, whereas cpSRP43 is not (Amin et al., 1999; Nilsson et al., 1999; Walter et al., 2015).

Regardless of their precise nature, the roles of the STIC proteins in thylakoid protein transport must be such that they can, if necessary, be compensated for by other factors, as the *stic* mutants do not display severe thylakoid defects. It will be necessary to identify the substrates of the STIC proteins before we can fully understand their roles and elucidate how their loss results in the suppression of *tic40*.

What Is the Functional Relationship between the STIC Proteins and Tic40?

It has long been assumed that Tic40 functions as part of a protein import motor, along with Tic110 and Hsp93 (Chou et al., 2003, 2006; Kovacheva et al., 2005). However, the absence of these components from the newly identified 1 MD TIC complex cast some doubt on this model (Kikuchi et al., 2013). The recent finding that Hsp93 may perform a protein quality control role during import, in partnership with the ClpP protease (Flores-Pérez et al., 2016), with Hsp70 performing the motor function instead (Shi and Theg, 2010; Su and Li, 2010), suggests that Tic40 may function immediately downstream of import rather than during the import process per se. This view fits well with the hypothesis that Tic40 participates in the postimport targeting of proteins to the inner envelope and thylakoids (Chiu and Li, 2008; Ouyang et al., 2011).

Assuming that Tic40 plays a key role in sorting as proteins exit the import process, its loss may be accompanied not only by the disruption of import (Chou et al., 2003; Kovacheva et al., 2005), but also by the mistargeting of certain proteins. For example, proteins normally targeted to the inner envelope or thylakoids may enter noncognate targeting pathways with nonproductive outcomes in the absence of Tic40. If such mistargeting leads to thylakoid membranes that are held in close physical proximity to the TIC channel, further blockage of import may result. It is conceivable that STIC1/ALB4 and STIC2 act in such a noncognate pathway and that their loss causes a reduction in mistargeting events leading to partial suppression of the deleterious effects of *tic40* on protein transport and plant development.

A Link between Chloroplast Swelling, Plastoglobule Accumulation, and Loss of Membrane Integrity?

Intriguingly, the swollen appearance of the *tic40* chloroplasts and the accumulation of plastoglobules are largely unaffected in the suppressor mutants (Figure 1), and these are particular characteristics that *tic40* happens to share with both *stic* single mutants

(Figure 4) and which are not generally seen in other import-defective mutants (e.g., *ppi1*) (Jarvis et al., 1998). This phenotype is very similar to one observed upon moderate heat stress (40°C) treatment of Arabidopsis leaves, which is partially reversed after only 30 min of recovery, suggesting that the effect is primarily physicochemical in nature (Zhang et al., 2010). Moderate heat stress may cause increased membrane fluidity and, thus, greater proton leakage into the stroma, leading to acidification, osmotic stress, and organelle swelling.

Interestingly, a *vipp1* mutant was also reported to display a swollen chloroplast phenotype with disorganized, "ruffled" thylakoids (the VIPP1 protein, like its bacterial ortholog PspA, plays an important role in membrane maintenance) (Vothknecht et al., 2012; Zhang et al., 2012). In this mutant, spherical chloroplast morphology was linked to increased osmotic pressure inside the organelles, as the chloroplasts could be returned to their normal elliptical shape by increasing the osmotic concentration of the cytosol (Zhang et al., 2012). Again, the hypertonic state of the chloroplasts was attributed to membrane leakiness. Thus, it is conceivable that the chloroplast swelling seen in *tic40* occurs due to defects in inner envelope and/or thylakoid membrane integrity, while the less drastic swollen chloroplast phenotype seen in the *stic* single mutants may be associated with an effect on the thylakoid membranes only. The latter is supported by data showing reduced photosynthetic performance in *alb4* mutants (Benz et al., 2009; Trösch et al., 2015).

Plastoglobules are structures formed on thylakoid membranes that contain lipids (carotenoids, plastoquinone, and tocopherols) as well as lipid biosynthesis enzymes such as tocopherol cyclase (Steinmüller and Tevini, 1985; Austin et al., 2006). They are commonly observed in mutants with defects in thylakoid membrane biogenesis (e.g., *var2*) and following various biotic and abiotic stresses (Takechi et al., 2000; Bréhélin et al., 2007; Bréhélin and Kessler, 2008), and may be a mechanism to temporarily store lipids (e.g., tocopherols) in order to protect the thylakoid membranes from oxidative damage. Thus, the plastoglobule accumulation seen in the *tic40* and *stic* mutants is consistent with our hypothesis that these mutants experience membrane instability and leakage.

Tocopherol biosynthesis is initiated in the inner envelope membrane (Froehlich et al., 2003; Motohashi et al., 2003), so plastoglobules were suggested to form a metabolic link between the envelope and thylakoids (Ytterberg et al., 2006). Our observation that *stic1* and *stic2* (mutants that result in thylakoid biogenesis defects) can suppress *tic40* reveals a further link between the two membrane systems and sheds new light on the interconnectedness of protein import and thylakoid protein biogenesis. We expect that the *stic* mutants will provide an invaluable resource for further investigations on how these crucial processes are coordinated in the future.

METHODS

Plant Materials and Growth Conditions

Arabidopsis (*Arabidopsis thaliana*) Columbia-0 (Col-0) ecotype was employed as the wild type since the original, previously characterized *tic40-4* (SAIL_192_C10) mutant (Kovacheva et al., 2005) and the other T-DNA mutants used in this study are all in this background. The *stic1* and *stic2* T-DNA mutants, *alb4-1* (SALK_136199), *stic2-3* (SALK_001500), and *stic2-4* (WiscDsLox445D01), were all identified using the T-DNA Express website provided by the Salk Institute Genomic Analysis Laboratory (SIGnAL) and obtained from the Nottingham Arabidopsis Stock Centre or the ABRC (Alonso et al., 2003; Woody et al., 2007). The mutants *tic40-3* (Koncz line N33230), *tic110-1* (SAIL_896_D08), *hsp93-V-1* (SAIL_873_G11) (Kovacheva et al., 2005), *ppi1* (Jarvis et al., 1998), and *toc75-III-3* (*mar1*; introgressed into the Col-0 ecotype) (Stanga et al., 2009; Huang et al., 2011) were all previously described. The thylakoid targeting pathway component mutants *cpsrp54-3* (WiscDsLox289_292B14), *cpftsY-1* (SALK_049077), *cpftsY-2* (SALK_112451), and *secA-1* (SALK_063371) were also previously characterized (Asakura et al., 2008; Liu et al., 2010; Yu et al., 2012). To our knowledge, the *hcf106* (SALK_020680) mutant has not been characterized before, but it does produce a similar albino phenotype to a previously reported mutant of another Tat pathway component, TatC (Motohashi et al., 2001), while the *cpsrp43-2* (SAIL_783_F08) mutant (Sessions et al., 2002) was shown in this study to accumulate no detectable cpSRP43 protein.

The only instance where another ecotype was used was in the generation of hybrid mapping populations, where the *stic tic40-4* mutants were crossed with Landsberg *erecta* plants in which the *tic40-4* mutation had been introgressed; this was done by sequential backcrossing (10 times) of the original *tic40-4* Col-0 mutant with Landsberg *erecta* ecotype plants.

In vitro-grown plants were generally grown on Murashige and Skoog (MS) plant growth media (0.5–1× MS salts, 0.5% [w/v] sucrose, 0.05% [w/v] MES-KOH pH 5.7, and 0.6% [w/v] phytoagar). However, very chlorotic mutant seedlings (*cpsecA-1*, *hcf106*, and *cpftsY-1/2*) were usually transplanted to 3% (w/v) sucrose MS media, after ~10 d on normal media, for further growth. Plants on MS media were grown in Percival growth chambers with ~100 μmol m^{-2} s^{-1} fluorescent tube lighting (Philips) at 20°C under long-day (16 h light, 8 h dark) conditions. Seeds were sterilized by shaking for 5 min in 70% (v/v) ethanol containing 0.05% (v/v) Triton X-100, followed by shaking for 10 min in 100% ethanol, and then air-dried on sterile filter paper prior to sowing on MS media. Seeds on MS media were stratified for 2 d at 4°C before being transferred to the growth chamber. Normally, plants were transferred to soil after ~10 d of growth on MS media and kept either in growth cabinets, controlled environment rooms, or greenhouses under long-day (16 h light, 8 h dark) conditions. Chlorophyll measurements were performed using a SPAD-502 meter (Konica Minolta) using soil-grown plants as described previously (Ling et al., 2011).

When necessary, the following antibiotics were included in the medium at the indicated concentrations: 50 μg/mL of kanamycin monosulfate (Melford Laboratories) was used to select for the SALK T-DNA insertion lines; 10 μg/mL of DL-phosphinothricin (Duchefa) was used to select for SAIL and WiscDsLox lines; and 15 μg/mL of hygromycin B (Duchefa) was used for transgenics generated with the pH2GW7-FLAG plasmid.

Characterization of the *stic* T-DNA Mutants

To confirm the position of the T-DNA insertion in each *stic2* T-DNA mutant (*stic2-3* and *stic2-4*), the upstream flanking sequence of the insertion in each case was amplified using primers specific for the T-DNA left border (LB) and for the *STIC2* gene. In the case of *stic2-3*, primer SALK LBb1 (5′-GCGTGGACCGCTTGCTGCAACT-3′) was used in combination with the forward primer Stic2 Pro F (5′-CCTTTGTTAGGTCATGAC-3′), which binds upstream of the *STIC2* coding sequence (CDS; in the putative promoter region). In the case of *stic2-4*, the LB-specific primer WiscDsLox LB (p745) (5′-AACGTCCGCAATGTGTTATTAAGTTGTC-3′) was used in combination with the forward primer T29E15.22 F1 (5′-GCTTCCGGTTTTATCTTCTCG-3′). The PCR products obtained were cloned and sequenced to obtain precise positions of insertion (Figure 2B). For the *stic2-4* T-DNA mutant, the downstream T-DNA flanking sequence was also amplified with

the LB-specific primer in combination with T29E15.22 R3 (5′-GAACACGTACAGCTTCCACTTG-3′). Therefore, in this case, the LB is found on each side of the insertion site, indicating that the plant contains an inverted repeat T-DNA insertion. However, for the *stic2-3* T-DNA mutant, we failed to amplify the downstream flanking T-DNA sequence with either RB or LB primers, indicating that in this case the inserted T-DNA is likely truncated. For routine genotyping, the initial primer combinations were used to detect the insertion, and in each case the forward primer was used with the reverse primer T29E15.22 R3 to detect the wild-type *STIC2* gene. We proceeded to confirm that these T-DNA insertion lines segregated 3:1 for kanamycin (*stic2-3*) or phosphinothricin (*stic2-4*) resistance to ensure that they each contained just a single T-DNA insertion.

In the case of the *alb4-1* T-DNA insertion mutant, the position of the T-DNA was reported previously (Gerdes et al., 2006; Trösch et al., 2015). The mutant was routinely genotyped using the T-DNA-specific primer pair seqALB4-2-F (5′-CCTTGCAGGTACAGTATGTTA-3′) + SALK LBb1 and the genomic primer pair seqALB4-2-F + seqALB4-2-R (5′-CTGTTGCATAGAAGGATTTCG-3′) to detect the wild-type *STIC1* gene.

Constructs and Vectors Used for in Vivo Studies

The CDSs of *ALB3*, *STIC1/ALB4*, *STIC2*, and *STCL* were amplified from wild-type cDNA (*ALB3* and *STIC1/ALB4*) or obtained from the ABRC (cDNA clones: NM_001202657, *STIC2*; NM_119208, *STCL*). They were amplified to engineer AttB1 and AttB2 Gateway recombination sites at their 5′ and 3′ ends, respectively, without a stop codon, and were then cloned into the pDONR201 Gateway entry vector using Gateway technology (Invitrogen, ThermoFisher).

Coding sequences were amplified using Phusion high-fidelity DNA polymerase (New England Biolabs) with the following primer combinations: *ALB3*, ALB3-AttB1-F (5′-AAAAAGCAGGCTCCCACCAGCTTCGTCTCTCATTT-3′) + ALB3-AttB2-R (5′-AGAAAGCTGGGTTTACAGTGCGTTTCCGCTTCGA-3′); *ALB4*, ALB4-AttB1-F (ALB4-pENTR-F) (5′-AAAAAGCAGGCTCCCAAAGCAAGAACACAACAACA-3′) + ALB4-AttB2-R (ALB4-pENTR-R1) (5′-AGAAAGCTGGGTTCCTCTTCTCTGTTTCATGAGA-3′); *STIC2*, STIC2-AttB1-F (5′-AAAAGCAGGCTATGGCTGCAACCACCAT-3′) + STIC2-AttB2-R (5′-AGAAAGCTGGGTTCTTCATTCCTTCGCTGAG-3′); and *STCL*, STCL-AttB1-F (5′-AAAAAGCAGGCTATGGCTTCGACGGCTACG-3′) + STCL-AttB2-R (5′-AGAAAGCTGGGTTCTTTAATCCATCAAGGCC-3′). Another *STCL* CDS clone carrying its stop codon (STCL-CDS-STOP) was also amplified using STCL-AttB1-F + STCL-stop-AttB2-R (5′-AGAAAGCTGGGTTACTTTAATCCATCAAGGC-3′). The forward primer used to generate the *STIC2* CDS was designed to start at the second in-frame methionine codon and resulted in the loss of three amino acids from the transit peptide of the full STIC2 protein.

The CDS PCR products were further amplified with the AttB1/B2 primer pair (AttB1, 5′-GGGGACAAGTTTGTACAAAAAGCAGGCT-3′; AttB2, 5′-GGGGACCACTTTGTACAAGAAAGCTGGGT-3′) to add the full AttB recombination sequences prior to cloning. The *ALB3*, *ALB4*, *STIC2*, and *STCL* CDS inserts were then subcloned into the C-terminal YFP tag vector p2GWY7 (Karimi et al., 2002) to produce the ALB3-YFP, ALB4-YFP, STIC2-YFP, and STCL-YFP constructs, respectively. Also, the ALB4-CDS, STIC2-CDS, and STCL-CDS-STOP inserts were cloned into the C-terminal FLAG tag vector pH2GW7-FLAG, a vector derived from the original pH2GW7 vector (Karimi et al., 2002, 2005); the pH2GW7-FLAG vector was built by replacing the original Gateway cassette and 35S tobacco mosaic virus terminator of pH2GW7 with the Gateway cassette followed by a C-terminal FLAG tag and the octopine synthase terminator from the pEarleyGate302 (Earley et al., 2006). The YFP constructs were used for transient expression in protoplasts, while the FLAG constructs were used for stable, *Agrobacterium tumefaciens*-mediated transformation of wild-type and *stic1-1 tic40-4* (with ALB4-FLAG) or *stic2-1 tic40-4* (with STIC2-FLAG or STCL-CDS-STOP) plants. Arabidopsis plants were transformed by Agrobacterium infiltration using the previously described floral dip method (Clough and Bent, 1998). The Tic110-YFP construct used as controls for protoplast transfection in the localization studies (Figure 3) was described previously (Bédard et al., 2007).

Concerning the BiFC experiments, the ALB3, ALB4, and PSI-D constructs used were previously described (Trösch et al., 2015). In addition, new ALB4-G397S-cYFP, STIC2-nYFP, and STIC2-cYFP constructs were generated. For the ALB4-G397S-cYFP construct, the C terminus of the ALB4 protein was amplified from cDNA prepared from the *stic1-2* mutant with the primer combination ALB4-HIS-F (5′-GGGGGATCCCCAGTGGAGAAATTCACTAA-3′) + ALB4-SalI-BiFC-R (5′-AAGGTCGACTCCTCCTCTCTGTTTCATGAGA-3′), using Phusion high-fidelity DNA polymerase (New England Biolabs). The obtained PCR fragment was cut at the internal *Spe*I restriction site upstream of the point mutation responsible for the G397S substitution and the *Sal*I site added by the ALB4-SalI-BiFC-R primer, and the resulting *Spe*I-*Sal*I fragment was used to replace the corresponding fragment in the original ALB4-cYFP vector (Trösch et al., 2015). For the STIC2-nYFP and STIC2-cYFP constructs, the *STIC2* CDS was amplified using the primer combination STIC2-XhoI-BiFC-F (5′-AACTCGAGCATGGCGTCGATGGCTGCAAC-3′) + STIC2-HindIII-BiFC-R (5′-CCAAGCTTTTCATTCCTTCGCTGAGACC-3′) using Phusion DNA polymerase. After digestion of the PCR product with *Xho*I and *Hind*III, the resulting *STIC2* fragment was transferred into *Xho*I- and *Hind*III-cut pSAT4(A)-nEYFP-N1 and pSAT4(A)-cEYFP-N1 vectors (Tzfira et al., 2005) using standard molecular biology techniques.

Recombinant Protein Expression and STIC2 Antibody Production

The vector used here to express the soluble, 154-residue ALB4 C-terminal domain with an N-terminal 6xHis tag (His-ALB4C) was previously described and used to produce the ALB4 antibody (Trösch et al., 2015). The His-ALB4C-G397C expression vector is essentially equivalent, except that the ALB4 coding sequence was amplified from *stic1-2* mutant cDNA and carries the point mutation resulting in the G397C substitution. The His-ALB3C clone was produced by amplifying the coding sequence for the C-terminal 102 residues of ALB3 from wild-type cDNA using the following primers: ALB3-His-F (5′-AAGGATCCAATATGGATGGATGAAAACGCAAGC-3′) + ALB3-His-R (5′-TCGTCGACCTATACAGTGCGTTTCCGCT-3′). The obtained PCR fragment was digested with *Bam*HI and *Sal*I and cloned into the pQE-30 expression vector (Qiagen). The His-ALB4C, His-ALB4C-G397S, and His-ALB3C fusions were all expressed in XL1-Blue *Escherichia coli* cells (Agilent Technologies) grown in medium containing 0.4% (w/v) glucose followed by induction with 1 mM isopropyl β-D-1-thiogalactopyranoside (IPTG). The construct used to produce His-LTD (in the pET28a vector) was previously described (Ouyang et al., 2011).

The CDS encoding the predicted mature form of STIC2 (i.e., amino acids 49 to 182) was amplified using the primers STIC2-GST-2-F (5′-AAGGATCCGTGAATGGATTATTTG-3′) and STIC2-C-SalI-R (5′-AAGTCGACCCTTCATTCCTTCGCTG-3′) and transferred to the pGEX-6P1 as a *Bam*HI-*Sal*I fragment to produce the GST-STIC2 fusion. The GST-STIC2 construct was expressed in BL21 *E. coli* cells and induced with 0.2 mM IPTG, and the protein was purified from bacterial lysate produced by sonication in lysis buffer (50 mM NaH_2PO_4 and 300 mM NaCl, pH 8.0). Lysate was applied to polypropylene columns containing glutathione agarose resin (Sigma-Aldrich), before washing with wash buffer (50 mM NaH_2PO_4 and 300 mM NaCl, pH 8.0) and protein elution by cleavage overnight at 4°C with PreScission protease (GE Healthcare) in cleavage buffer (50 mM Tris-HCl, pH 7.0, 150 mM NaCl, 1 mM EDTA, 1 mM DTT, and 0.01% [v/v] Triton X-100). The purified protein was sent to Harlan Sera-lab for antibody production in rabbits, and the antiserum was affinity purified using the original antigen.

Seedling Protein Extractions and Immunoblotting

Total protein extracts were prepared using a modified, previously described procedure (Kovacheva et al., 2005). Briefly, 100 mg of 10- to 14-d-old seedlings was collected in a 2-mL Eppendorf tube, frozen in liquid nitrogen, and homogenized with a 5-mm stainless steel bead using a TissueLyser (Qiagen) by shaking at 12,000 rpm for 1 min. After pelleting the resulting tissue powder (pulse spin at 20,000*g* and 4°C), 0.2 mL protein extraction buffer (100 mM Tris-HCl, pH 6.8, 10% [v/v] glycerol, 2% [w/v] SDS, 1% [v/v] Triton X-100, 100 mM DTT, and 1× plant protease inhibitor cocktail [Sigma-Aldrich]) was added before mixing at 1400 rpm and 4°C for 20 to 30 min in a Thermomixer (Eppendorf). After spinning down the insoluble material (10 min at 20,000*g*), the supernatant was transferred to a new tube and a Bradford assay kit (Bio-Rad) was used to measure the protein concentration. Samples of equal protein concentration were prepared and used for analysis. SDS-PAGE and immunoblotting using PVDF (Millipore) membranes were performed employing standard procedures.

Transmission Electron Microscopy

For transmission electron microscopy, the cotyledons from 10-d-old plants were used. The tissue was prepared and imaged with the help of the University of Leicester Electron Microscope Laboratory (Faculty of Medicine and Biological Sciences). Cotyledons were excised from in vitro-grown seedlings and fixed overnight in 4% (v/v) glutaraldehyde/2% (v/v) formaldehyde in 0.1 M sodium cacodylate buffer with 2 mM calcium chloride (pH 7.2) and then washed in the same cacodylate/$CaCl_2$ buffer. The tissue was then fixed with 1% (w/v) OsO_4/1.5% (w/v) potassium ferricyanide for 3 h, washed with distilled, deionized water, and finally tertiary-fixed with 2% (w/v) uranyl acetate for 1 h. The tissue was serially dehydrated through ethanol and propylene oxide and embedded in Spurr's modified low viscosity resin. Thin sections of ~80 nm thickness were cut using a Reichert Ultracut S ultramicrotome, collected onto copper mesh grids, and stained with Reynolds' lead citrate. The grids were viewed under a JEOL JEM-1400 electron microscope at 80 kV. Digital images were recorded using a SIS digital camera and iTEM software (Glauert and Lewis, 1998; Hyman and Jarvis, 2011).

Protoplast Transfection and Microscopy for Localization and BiFC Interaction Assays

Protoplasts from 4- to 5-week-old wild-type plants grown on soil were isolated using the tape Arabidopsis-sandwich method (Wu et al., 2009). Approximately10^5 protoplasts and 5 μg of plasmid DNA were used per (co)transfection in 40% (w/v) PEG-4000 solution (Wu et al., 2009). Samples were analyzed 16 to 18 h after (co)transfection using a Zeiss LSM 510 META confocal laser scanning microscope and a C-Apochromat 40×/1.2-W Corr. objective. To detect YFP, 514-nm excitation from a 5-mW argon ion laser with an HFT 458/514 primary dichroic mirror and a 535- to 590-nm emission filter was used. To simultaneously detect chlorophyll autofluorescence, an NFT 635 visual long-pass filter was used. Images were processed with Zeiss LSM Image Browser software. Each (co)transfection was conducted three times, with the same result, and typical images are shown.

Chloroplast Isolation, Subfractionation, and Import Assays

Chloroplasts were isolated from 10- to 14-d-old in vitro-grown Arabidopsis seedlings as previously described (Aronsson and Jarvis, 2011). Chloroplasts were lysed hypotonically and subfractionated into soluble (stroma and intermembrane space), envelope, and thylakoid fractions by sucrose density gradient centrifugation as previously described (Flores-Pérez and Jarvis, 2017). In vitro chloroplast protein import assays were performed as described previously (Aronsson and Jarvis, 2011).

Co-IP Experiments

Chloroplasts were isolated from 14-d-old, in vitro-grown wild-type and STIC1-FLAG- or STIC2-FLAG-expressing seedlings. Amounts of chloroplasts equivalent to 0.4 mg of chlorophyll were cross-linked with 250 or 500 μM DSP (or mock-treated without DSP) on ice for 15 min in HMS buffer (50 mM HEPES-NaOH, pH 8.0, 3 mM $MgSO_4$, and 0.33 M sorbitol). The DSP was then quenched by adding glycine (in HMS) to a final concentration of 50 mM, and the chloroplasts were further incubated on ice for 30 min after mixing. Chloroplast samples were split into two 0.2 mg chlorophyll aliquots, pelleted by spinning for 1 min at 10,000*g*, and frozen in liquid nitrogen. Chloroplast pellets of 0.2 mg chlorophyll were solubilized in 1.5 mL dodecyl maltoside (DDM) solubilization buffer (SB) (50 mM Tris-HCl, pH 7.4, 1% [w/v] DDM, 150 mM NaCl, 1 mM EDTA, 10% [v/v] glycerol, and 1× plant protease inhibitor cocktail [Sigma-Aldrich]) by rotating at 4°C for 1 h. The insoluble material was removed by centrifugation at 20,000*g* for 10 min at 4°C, and then the supernatants were mixed with 25 μL of preequilibrated anti-FLAG resin (Sigma-Aldrich) in a micro-spin column (Bio-Rad) by rotation for 2 h at 4°C. The resin was then pelleted by centrifugation at 500*g* for 1 min, and the flow-through was collected. The resin was washed twice with 0.5 mL of SB, and six times with 0.5 mL of wash buffer (SB with 0.1% [w/v] DDM instead of 1% [w/v] DDM). Bound proteins were eluted using 98 μL of SDS sample buffer without DTT (100 mM Tris-HCl, pH 6.8, 10% [v/v] glycerol, 2% [w/v] SDS, 1% [v/v] Triton X-100, 0.05% [w/v] bromophenol blue dye, and 1× plant protease inhibitor cocktail [Sigma-Aldrich]) by heating at 90°C and shaking at 600 rpm in a Thermomixer for 10 min. The eluate was then supplemented with 2 μL of 1 M DTT.

In Vitro Pull-Down Experiments

Recombinant His-tagged and GST-tagged proteins were expressed in 50 mL bacterial cultures induced with 0.2 to 1.0 mM IPTG. Bacterial lysates were prepared in 5 mL lysis buffer (50 mM Tris-HCl, pH 7.5, 150 mM NaCl, 10 mM imidazole, 0.01% [v/v] Triton X-100, 0.05 mg/mL lysozyme, and 1× Complete EDTA-free protease inhibitor cocktail [Roche Diagnostics]) from frozen bacterial pellets. Equal amounts (0.5 mL) of bacterial lysates from His-tag and GST-tag expressors were combined and mixed with 25 to 50 μL of Ni-NTA resin (Qiagen) in a micro-spin column (Bio-Rad) for 2 h by rotation at 4°C. The resin was pelleted by centrifugation at 500*g* for 1 min, and the flow-through was collected. The resin was then washed four to five times with 0.5 mL wash buffer (50 mM Tris-HCl, pH 7.5, 150 mM NaCl, and 20 mM imidazole). Bound proteins were eluted by washing four times with 50 μL of elution buffer (50 mM Tris-HCl, pH 7.5, 150 mM NaCl, 250 mM imidazole, and 10% [v/v] glycerol), and each eluate was mixed with 15 μL 5× SDS sample buffer (500 mM Tris-HCl, pH 6.8, 50% [v/v] glycerol, 10% [w/v] SDS, 5% [v/v] Triton X-100, and 500 mM DTT). After electrophoresis, stained bands were quantified using ImageJ software (Schneider et al., 2012).

Accession Numbers

The following gene codes can be used to access the full-length gene, cDNA, CDS, and protein sequences from TAIR: At1g24490 (*STIC1/ALB4*), At2g24020 (*STIC2*), and At4g30620 (*STCL*). For protein alignments, we used the STIC2 (NP_001189586) and STCL (NP_194791) sequences from the GenBank database. The STIC2 homologs used in the phylogenetic analysis are listed in Supplemental Data Set 2.

Supplemental Data

Supplemental Figure 1. The selected suppressor mutants carry semidominant mutations.

Supplemental Figure 2. Cotyledon cell architecture in the suppressed *stic tic40* double mutant seedlings.

Supplemental Figure 3. Identification of *stic1* and *stic2* loci by map-based cloning.

Supplemental Figure 4. RT-PCR analysis of the expression of *STIC1* and *STIC2* in the *stic* mutants.

Supplemental Figure 5. Phenotypic comparisons of the different *stic1* and *stic2* alleles.

Supplemental Figure 6. Complementation of the *stic* mutations by STIC-FLAG overexpression constructs.

Supplemental Figure 7. Analysis of the Arabidopsis STIC2 homolog, STIC2 Like.

Supplemental Figure 8. Phylogenetic analysis of STIC2/STCL sequences from plant and bacterial species.

Supplemental Figure 9. Analysis of *stic2 stcl* double mutants generated using a *STCL* amiRNA construct.

Supplemental Figure 10. Analysis of the localization of ALB4 at different stages of development.

Supplemental Figure 11. Specificity of the suppression effects of the *stic1* and *stic2* mutations.

Supplemental Figure 12. Immunoblot analysis of the cpSRP pathway mutants and phenotypes of the *stic cpsrp43* double mutants.

Supplemental Figure 13. Control images for the in vivo analysis of interactions between STIC2 and the STIC1/ALB4 and ALB3 proteins.

Supplemental Figure 14. Structural models showing surface electrostatic potential of STIC2 and STCL relative to the *E. coli* homolog YbaB.

Supplemental Methods.

Supplemental Data Set 1. Alignment of the sequences of the STIC2/STCL-type proteins used in the phylogenetic analysis.

Supplemental Data Set 2. Sequences of STIC2/STCL-type proteins used in the phylogenetic analysis.

ACKNOWLEDGMENTS

We thank Natalie Allcock and Stefan Hyman at the University of Leicester Electron Microscope Laboratory for the imaging by light and transmission electron microscopy of cotyledon cross sections and chloroplasts. We also thank Madeleine Rashbrooke for assisting with the mapping of the *stic* loci. We acknowledge Masato Nakai for kindly providing seeds of the *cpftsY-1* and *cpftsY-2* Arabidopsis mutants and Lixing Zhang for his gift of the His-LTD expression vector. Excellent technical assistance in plant handling, growth and genotyping was provided by Ramesh Patel and Sean Maguire. We acknowledge financial support from the Biotechnology and Biological Sciences Research Council (grant numbers BB/J009369/1, BB/J017256/1, BB/C006348/1, and 91/C18638) (to P.J.), from the Royal Society Rosenheim Research Fellowship (to P.J.), by a Royal Society Sino-British Fellowship Trust (SBFT) Postdoctoral Fellowship (to F.W.), by a Gatsby Charitable Foundation Sainsbury PhD Studentship (to R.T.), by a Universities UK Overseas Research Students (ORS) Award (to J.B.), and by a European Commission Erasmus Mundus EXPERTS4Asia Scholarship (to F.N.).

AUTHOR CONTRIBUTIONS

J.B. conducted the mutant screen and identified the *stic* mutants, carried out the initial characterization of the mutants, identified the *stic2* locus, participated in the functional analysis of the STIC1/ALB4, STIC2, and STCL proteins, and drafted the manuscript. R.T. identified the *stic1* locus, participated in the functional analysis of the STIC1/ALB4 and STIC2 proteins, and contributed significantly to the preparation of the manuscript. F.W. contributed to the functional analysis of the STIC1/ALB4, STIC2, and STCL proteins. Q.L. contributed to the genetic analyses of the mutants and the YFP localization studies, and critically read the manuscript. Ú.F.-P. carried out the BiFC interaction analyses and critically read the manuscript. M.T. performed the phylogenetic analysis. F.N. contributed to the in vitro pull-down interaction studies. P.J. helped with the design of the experiments, supervised the project, and critically read and edited the manuscript.

Received January 4, 2017; revised June 2, 2017; accepted July 2, 2017; published July 6, 2017.

REFERENCES

Akita, M., Nielsen, E., and Keegstra, K. (1997). Identification of protein transport complexes in the chloroplastic envelope membranes via chemical cross-linking. J. Cell Biol. **136:** 983–994.

Alonso, J.M., et al. (2003). Genome-wide insertional mutagenesis of *Arabidopsis thaliana*. Science **301:** 653–657.

Amin, P., Sy, D.A., Pilgrim, M.L., Parry, D.H., Nussaume, L., and Hoffman, N.E. (1999). *Arabidopsis* mutants lacking the 43- and 54-kilodalton subunits of the chloroplast signal recognition particle have distinct phenotypes. Plant Physiol. **121:** 61–70.

Aoki, Y., Okamura, Y., Tadaka, S., Kinoshita, K., and Obayashi, T. (2016). ATTED-II in 2016: A plant coexpression database towards lineage-specific coexpression. Plant Cell Physiol. **57:** e5.

Aronsson, H., and Jarvis, R.P. (2011). Rapid isolation of Arabidopsis chloroplasts and their use for in vitro protein import assays. Methods Mol. Biol. **774:** 281–305.

Asakura, Y., Kikuchi, S., and Nakai, M. (2008). Non-identical contributions of two membrane-bound cpSRP components, cpFtsY and Alb3, to thylakoid biogenesis. Plant J. **56:** 1007–1017.

Austin II, J.R., Frost, E., Vidi, P.A., Kessler, F., and Staehelin, L.A. (2006). Plastoglobules are lipoprotein subcompartments of the chloroplast that are permanently coupled to thylakoid membranes and contain biosynthetic enzymes. Plant Cell **18:** 1693–1703.

Balsera, M., Goetze, T.A., Kovács-Bogdán, E., Schürmann, P., Wagner, R., Buchanan, B.B., Soll, J., and Bölter, B. (2009). Characterization of Tic110, a channel-forming protein at the inner envelope membrane of chloroplasts, unveils a response to Ca(2+) and a stromal regulatory disulfide bridge. J. Biol. Chem. **284:** 2603–2616.

Bédard, J., Kubis, S., Bimanadham, S., and Jarvis, P. (2007). Functional similarity between the chloroplast translocon component, Tic40, and the human co-chaperone, Hsp70-interacting protein (Hip). J. Biol. Chem. **282:** 21404–21414.

Bellafiore, S., Ferris, P., Naver, H., Göhre, V., and Rochaix, J.D. (2002). Loss of Albino3 leads to the specific depletion of the light-harvesting system. Plant Cell **14:** 2303–2314.

Benz, M., Bals, T., Gügel, I.L., Piotrowski, M., Kuhn, A., Schünemann, D., Soll, J., and Ankele, E. (2009). Alb4 of *Arabidopsis* promotes assembly and stabilization of a non chlorophyll-binding photosynthetic complex, the CF_1CF_0-ATP synthase. Mol. Plant **2:** 1410–1424.

Berendzen, K., Searle, I., Ravenscroft, D., Koncz, C., Batschauer, A., Coupland, G., Somssich, I.E., and Ulker, B. (2005). A rapid and versatile combined DNA/RNA extraction protocol and its application to the analysis of a novel DNA marker set polymorphic between

Arabidopsis thaliana ecotypes Col-0 and Landsberg *erecta*. Plant Methods **1:** 4.

Bréhélin, C., and Kessler, F. (2008). The plastoglobule: a bag full of lipid biochemistry tricks. Photochem. Photobiol. **84:** 1388–1394.

Bréhélin, C., Kessler, F., and van Wijk, K.J. (2007). Plastoglobules: versatile lipoprotein particles in plastids. Trends Plant Sci. **12:** 260–266.

Celedon, J.M., and Cline, K. (2013). Intra-plastid protein trafficking: how plant cells adapted prokaryotic mechanisms to the eukaryotic condition. Biochim. Biophys. Acta **1833:** 341–351.

Chen, X., Smith, M.D., Fitzpatrick, L., and Schnell, D.J. (2002). *In vivo* analysis of the role of atTic20 in protein import into chloroplasts. Plant Cell **14:** 641–654.

Chiu, C.C., and Li, H.M. (2008). Tic40 is important for reinsertion of proteins from the chloroplast stroma into the inner membrane. Plant J. **56:** 793–801.

Chou, M.L., Chu, C.C., Chen, L.J., Akita, M., and Li, H.M. (2006). Stimulation of transit-peptide release and ATP hydrolysis by a cochaperone during protein import into chloroplasts. J. Cell Biol. **175:** 893–900.

Chou, M.L., Fitzpatrick, L.M., Tu, S.L., Budziszewski, G., Potter-Lewis, S., Akita, M., Levin, J.Z., Keegstra, K., and Li, H.M. (2003). Tic40, a membrane-anchored co-chaperone homolog in the chloroplast protein translocon. EMBO J. **22:** 2970–2980.

Clough, S.J., and Bent, A.F. (1998). Floral dip: a simplified method for *Agrobacterium*-mediated transformation of *Arabidopsis thaliana.* Plant J. **16:** 735–743.

Cooley, A.E., Riley, S.P., Kral, K., Miller, M.C., DeMoll, E., Fried, M.G., and Stevenson, B. (2009). DNA-binding by *Haemophilus influenzae* and *Escherichia coli* YbaB, members of a widely-distributed bacterial protein family. BMC Microbiol. **9:** 137.

Demarsy, E., Lakshmanan, A.M., and Kessler, F. (2014). Border control: selectivity of chloroplast protein import and regulation at the TOC-complex. Front. Plant Sci. **5:** 483.

Dünschede, B., Bals, T., Funke, S., and Schünemann, D. (2011). Interaction studies between the chloroplast signal recognition particle subunit cpSRP43 and the full-length translocase Alb3 reveal a membrane-embedded binding region in Alb3 protein. J. Biol. Chem. **286:** 35187–35195.

Earley, K.W., Haag, J.R., Pontes, O., Opper, K., Juehne, T., Song, K., and Pikaard, C.S. (2006). Gateway-compatible vectors for plant functional genomics and proteomics. Plant J. **45:** 616–629.

Emanuelsson, O., Nielsen, H., Brunak, S., and von Heijne, G. (2000). Predicting subcellular localization of proteins based on their N-terminal amino acid sequence. J. Mol. Biol. **300:** 1005–1016.

Falk, S., Ravaud, S., Koch, J., and Sinning, I. (2010). The C terminus of the Alb3 membrane insertase recruits cpSRP43 to the thylakoid membrane. J. Biol. Chem. **285:** 5954–5962.

Flores-Pérez, Ú., and Jarvis, P. (2017). Isolation and suborganellar fractionation of Arabidopsis chloroplasts. Methods Mol. Biol. **1511:** 45–60.

Flores-Pérez, Ú., Bédard, J., Tanabe, N., Lymperopoulos, P., Clarke, A.K., and Jarvis, P. (2016). Functional analysis of the Hsp93/ClpC chaperone at the chloroplast envelope. Plant Physiol. **170:** 147–162.

Froehlich, J.E., Wilkerson, C.G., Ray, W.K., McAndrew, R.S., Osteryoung, K.W., Gage, D.A., and Phinney, B.S. (2003). Proteomic study of the *Arabidopsis thaliana* chloroplastic envelope membrane utilizing alternatives to traditional two-dimensional electrophoresis. J. Proteome Res. **2:** 413–425.

Gerdes, L., Bals, T., Klostermann, E., Karl, M., Philippar, K., Hünken, M., Soll, J., and Schünemann, D. (2006). A second thylakoid membrane-localized Alb3/OxaI/YidC homologue is involved in proper chloroplast biogenesis in *Arabidopsis thaliana.* J. Biol. Chem. **281:** 16632–16642.

Glauert, A.M., and Lewis, P.R. (1998). Biological Specimen Preparation for Transmission Electron Microscopy. (London: Portland Press).

Heins, L., Mehrle, A., Hemmler, R., Wagner, R., Küchler, M., Hörmann, F., Sveshnikov, D., and Soll, J. (2002). The preprotein conducting channel at the inner envelope membrane of plastids. EMBO J. **21:** 2616–2625.

Huang, P.K., Chan, P.T., Su, P.H., Chen, L.J., and Li, H.M. (2016). Chloroplast Hsp93 directly binds to transit peptides at an early stage of the preprotein import process. Plant Physiol. **170:** 857–866.

Huang, W., Ling, Q., Bédard, J., Lilley, K., and Jarvis, P. (2011). *In vivo* analyses of the roles of essential Omp85-related proteins in the chloroplast outer envelope membrane. Plant Physiol. **157:** 147–159.

Hyman, S., and Jarvis, R.P. (2011). Studying *Arabidopsis* chloroplast structural organisation using transmission electron microscopy. Methods Mol. Biol. **774:** 113–132.

Inaba, T., Li, M., Alvarez-Huerta, M., Kessler, F., and Schnell, D.J. (2003). atTic110 functions as a scaffold for coordinating the stromal events of protein import into chloroplasts. J. Biol. Chem. **278:** 38617–38627.

Inaba, T., Alvarez-Huerta, M., Li, M., Bauer, J., Ewers, C., Kessler, F., and Schnell, D.J. (2005). *Arabidopsis* Tic110 is essential for the assembly and function of the protein import machinery of plastids. Plant Cell **17:** 1482–1496.

Jackson, D.T., Froehlich, J.E., and Keegstra, K. (1998). The hydrophilic domain of Tic110, an inner envelope membrane component of the chloroplastic protein translocation apparatus, faces the stromal compartment. J. Biol. Chem. **273:** 16583–16588.

Jarvis, P. (2008). Targeting of nucleus-encoded proteins to chloroplasts in plants. New Phytol. **179:** 257–285.

Jarvis, P., Chen, L.J., Li, H., Peto, C.A., Fankhauser, C., and Chory, J. (1998). An *Arabidopsis* mutant defective in the plastid general protein import apparatus. Science **282:** 100–103.

Jutras, B.L., Bowman, A., Brissette, C.A., Adams, C.A., Verma, A., Chenail, A.M., and Stevenson, B. (2012). EbfC (YbaB) is a new type of bacterial nucleoid-associated protein and a global regulator of gene expression in the Lyme disease spirochete. J. Bacteriol. **194:** 3395–3406.

Kao, Y.F., Lou, Y.C., Yeh, Y.H., Hsiao, C.D., and Chen, C. (2012). Solution structure of the C-terminal NP-repeat domain of Tic40, a co-chaperone during protein import into chloroplasts. J. Biochem. **152:** 443–451.

Karimi, M., Inzé, D., and Depicker, A. (2002). GATEWAY vectors for *Agrobacterium*-mediated plant transformation. Trends Plant Sci. **7:** 193–195.

Karimi, M., De Meyer, B., and Hilson, P. (2005). Modular cloning in plant cells. Trends Plant Sci. **10:** 103–105.

Kelley, L.A., Mezulis, S., Yates, C.M., Wass, M.N., and Sternberg, M.J. (2015). The Phyre2 web portal for protein modeling, prediction and analysis. Nat. Protoc. **10:** 845–858.

Kikuchi, S., Bédard, J., Hirano, M., Hirabayashi, Y., Oishi, M., Imai, M., Takase, M., Ide, T., and Nakai, M. (2013). Uncovering the protein translocon at the chloroplast inner envelope membrane. Science **339:** 571–574.

Klimyuk, V.I., Persello-Cartieaux, F., Havaux, M., Contard-David, P., Schuenemann, D., Meiherhoff, K., Gouet, P., Jones, J.D., Hoffman, N.E., and Nussaume, L. (1999). A chromodomain protein encoded by the Arabidopsis *CAO* gene is a plant-specific component of the chloroplast signal recognition particle pathway that is involved in LHCP targeting. Plant Cell **11:** 87–99.

Konieczny, A., and Ausubel, F.M. (1993). A procedure for mapping *Arabidopsis* mutations using co-dominant ecotype-specific PCR-based markers. Plant J. **4:** 403–410.

Kovacheva, S., Bédard, J., Patel, R., Dudley, P., Twell, D., Ríos, G., Koncz, C., and Jarvis, P. (2005). *In vivo* studies on the roles of Tic110, Tic40 and Hsp93 during chloroplast protein import. Plant J. **41:** 412–428.

Krogh, A., Larsson, B., von Heijne, G., and Sonnhammer, E.L. (2001). Predicting transmembrane protein topology with a hidden Markov model: application to complete genomes. J. Mol. Biol. **305:** 567–580.

Kubis, S., Baldwin, A., Patel, R., Razzaq, A., Dupree, P., Lilley, K., Kurth, J., Leister, D., and Jarvis, P. (2003). The *Arabidopsis ppi1* mutant is specifically defective in the expression, chloroplast import, and accumulation of photosynthetic proteins. Plant Cell **15:** 1859–1871.

Kudla, J., and Bock, R. (2016). Lighting the way to protein-protein interactions: Recommendations on best practices for bimolecular fluorescence complementation analyses. Plant Cell **28:** 1002–1008.

Kuhn, A., Stuart, R., Henry, R., and Dalbey, R.E. (2003). The Alb3/Oxa1/YidC protein family: membrane-localized chaperones facilitating membrane protein insertion? Trends Cell Biol. **13:** 510–516.

Lee, L.Y., Fang, M.J., Kuang, L.Y., and Gelvin, S.B. (2008). Vectors for multi-color bimolecular fluorescence complementation to investigate protein-protein interactions in living plant cells. Plant Methods **4:** 24.

Leister, D. (2016). Towards understanding the evolution and functional diversification of DNA-containing plant organelles. F1000 Res. **5:** 330.

Li, H.M., and Chiu, C.C. (2010). Protein transport into chloroplasts. Annu. Rev. Plant Biol. **61:** 157–180.

Lim, K., Tempczyk, A., Parsons, J.F., Bonander, N., Toedt, J., Kelman, Z., Howard, A., Eisenstein, E., and Herzberg, O. (2003). Crystal structure of YbaB from *Haemophilus influenzae* (HI0442), a protein of unknown function coexpressed with the recombinational DNA repair protein RecR. Proteins **50:** 375–379.

Ling, Q., Huang, W., and Jarvis, P. (2011). Use of a SPAD-502 meter to measure leaf chlorophyll concentration in *Arabidopsis thaliana.* Photosynth. Res. **107:** 209–214.

Liu, D., Gong, Q., Ma, Y., Li, P., Li, J., Yang, S., Yuan, L., Yu, Y., Pan, D., Xu, F., and Wang, N.N. (2010). cpSecA, a thylakoid protein translocase subunit, is essential for photosynthetic development in *Arabidopsis.* J. Exp. Bot. **61:** 1655–1669.

Liu, L., McNeilage, R.T., Shi, L.X., and Theg, S.M. (2014). ATP requirement for chloroplast protein import is set by the K_m for ATP hydrolysis of stromal Hsp70 in *Physcomitrella patens.* Plant Cell **26:** 1246–1255.

Luirink, J., Samuelsson, T., and de Gier, J.W. (2001). YidC/Oxa1p/Alb3: evolutionarily conserved mediators of membrane protein assembly. FEBS Lett. **501:** 1–5.

Moore, M., Harrison, M.S., Peterson, E.C., and Henry, R. (2000). Chloroplast Oxa1p homolog albino3 is required for post-translational integration of the light harvesting chlorophyll-binding protein into thylakoid membranes. J. Biol. Chem. **275:** 1529–1532.

Motohashi, R., Nagata, N., Ito, T., Takahashi, S., Hobo, T., Yoshida, S., and Shinozaki, K. (2001). An essential role of a TatC homologue of a ΔpH-dependent protein transporter in thylakoid membrane formation during chloroplast development in *Arabidopsis thaliana.* Proc. Natl. Acad. Sci. USA **98:** 10499–10504.

Motohashi, R., Ito, T., Kobayashi, M., Taji, T., Nagata, N., Asami, T., Yoshida, S., Yamaguchi-Shinozaki, K., and Shinozaki, K. (2003). Functional analysis of the 37 kDa inner envelope membrane polypeptide in chloroplast biogenesis using a *Ds*-tagged *Arabidopsis* pale-green mutant. Plant J. **34:** 719–731.

Nilsson, R., Brunner, J., Hoffman, N.E., and van Wijk, K.J. (1999). Interactions of ribosome nascent chain complexes of the chloroplast-encoded D1 thylakoid membrane protein with cpSRP54. EMBO J. **18:** 733–742.

Ouyang, M., Li, X., Ma, J., Chi, W., Xiao, J., Zou, M., Chen, F., Lu, C., and Zhang, L. (2011). LTD is a protein required for sorting light-harvesting chlorophyll-binding proteins to the chloroplast SRP pathway. Nat. Commun. **2:** 277.

Paila, Y.D., Richardson, L.G., and Schnell, D.J. (2015). New insights into the mechanism of chloroplast protein import and its integration with protein quality control, organelle biogenesis and development. J. Mol. Biol. **427:** 1038–1060.

Pasch, J.C., Nickelsen, J., and Schünemann, D. (2005). The yeast split-ubiquitin system to study chloroplast membrane protein interactions. Appl. Microbiol. Biotechnol. **69:** 440–447.

Peltier, J.B., Ytterberg, A.J., Sun, Q., and van Wijk, K.J. (2004). New functions of the thylakoid membrane proteome of *Arabidopsis thaliana* revealed by a simple, fast, and versatile fractionation strategy. J. Biol. Chem. **279:** 49367–49383.

Rudella, A., Friso, G., Alonso, J.M., Ecker, J.R., and van Wijk, K.J. (2006). Downregulation of ClpR2 leads to reduced accumulation of the ClpPRS protease complex and defects in chloroplast biogenesis in Arabidopsis. Plant Cell **18:** 1704–1721.

Schneider, C.A., Rasband, W.S., and Eliceiri, K.W. (2012). NIH Image to ImageJ: 25 years of image analysis. Nat. Methods **9:** 671–675.

Schuenemann, D., Gupta, S., Persello-Cartieaux, F., Klimyuk, V.I., Jones, J.D., Nussaume, L., and Hoffman, N.E. (1998). A novel signal recognition particle targets light-harvesting proteins to the thylakoid membranes. Proc. Natl. Acad. Sci. USA **95:** 10312–10316.

Sessions, A., et al. (2002). A high-throughput *Arabidopsis* reverse genetics system. Plant Cell **14:** 2985–2994.

Shi, L.X., and Theg, S.M. (2010). A stromal heat shock protein 70 system functions in protein import into chloroplasts in the moss *Physcomitrella patens.* Plant Cell **22:** 205–220.

Shi, L.X., and Theg, S.M. (2013). The chloroplast protein import system: from algae to trees. Biochim. Biophys. Acta **1833:** 314–331.

Sjögren, L.L.E., Tanabe, N., Lymperopoulos, P., Khan, N.Z., Rodermel, S.R., Aronsson, H., and Clarke, A.K. (2014). Quantitative analysis of the chloroplast molecular chaperone ClpC/Hsp93 in *Arabidopsis* reveals new insights into its localization, interaction with the Clp proteolytic core, and functional importance. J. Biol. Chem. **289:** 11318–11330.

Skretas, G., and Georgiou, G. (2010). Simple genetic selection protocol for isolation of overexpressed genes that enhance accumulation of membrane-integrated human G protein-coupled receptors in *Escherichia coli.* Appl. Environ. Microbiol. **76:** 5852–5859.

Stanga, J.P., Boonsirichai, K., Sedbrook, J.C., Otegui, M.S., and Masson, P.H. (2009). A role for the TOC complex in *Arabidopsis* root gravitropism. Plant Physiol. **149:** 1896–1905.

Steinmüller, D., and Tevini, M. (1985). Composition and function of plastoglobuli: I. Isolation and purification from chloroplasts and chromoplasts. Planta **163:** 201–207.

Stengel, K.F., Holdermann, I., Cain, P., Robinson, C., Wild, K., and Sinning, I. (2008). Structural basis for specific substrate recognition by the chloroplast signal recognition particle protein cpSRP43. Science **321:** 253–256.

Su, P.H., and Li, H.M. (2010). Stromal Hsp70 is important for protein translocation into pea and *Arabidopsis* chloroplasts. Plant Cell **22:** 1516–1531.

Sun, Q., Emanuelsson, O., and van Wijk, K.J. (2004). Analysis of curated and predicted plastid subproteomes of *Arabidopsis*. Subcellular

compartmentalization leads to distinctive proteome properties. Plant Physiol. **135:** 723–734.

Sundberg, E., Slagter, J.G., Fridborg, I., Cleary, S.P., Robinson, C., and Coupland, G. (1997). *ALBINO3*, an *Arabidopsis* nuclear gene essential for chloroplast differentiation, encodes a chloroplast protein that shows homology to proteins present in bacterial membranes and yeast mitochondria. Plant Cell **9:** 717–730.

Takechi, K., Sodmergen, Murata, M., Motoyoshi, F., and Sakamoto, W. (2000). The *YELLOW VARIEGATED* (*VAR2*) locus encodes a homologue of FtsH, an ATP-dependent protease in *Arabidopsis.* Plant Cell Physiol. **41:** 1334–1346.

Teng, Y.S., Su, Y.S., Chen, L.J., Lee, Y.J., Hwang, I., and Li, H.M. (2006). Tic21 is an essential translocon component for protein translocation across the chloroplast inner envelope membrane. Plant Cell **18:** 2247–2257.

Tripp, J., Inoue, K., Keegstra, K., and Froehlich, J.E. (2007). A novel serine/proline-rich domain in combination with a transmembrane domain is required for the insertion of AtTic40 into the inner envelope membrane of chloroplasts. Plant J. **52:** 824–838.

Trösch, R., Töpel, M., Flores-Pérez, Ú., and Jarvis, P. (2015). Genetic and Physical Interaction Studies Reveal Functional Similarities between ALBINO3 and ALBINO4 in *Arabidopsis.* Plant Physiol. **169:** 1292–1306.

Tsai, J.Y., Chu, C.C., Yeh, Y.H., Chen, L.J., Li, H.M., and Hsiao, C.D. (2013). Structural characterizations of the chloroplast translocon protein Tic110. Plant J. **75:** 847–857.

Tu, C.J., Peterson, E.C., Henry, R., and Hoffman, N.E. (2000). The L18 domain of light-harvesting chlorophyll proteins binds to chloroplast signal recognition particle 43. J. Biol. Chem. **275:** 13187–13190.

Tzfira, T., Tian, G.W., Lacroix, B., Vyas, S., Li, J., Leitner-Dagan, Y., Krichevsky, A., Taylor, T., Vainstein, A., and Citovsky, V. (2005). pSAT vectors: a modular series of plasmids for autofluorescent protein tagging and expression of multiple genes in plants. Plant Mol. Biol. **57:** 503–516.

Tzvetkova-Chevolleau, T., et al. (2007). Canonical signal recognition particle components can be bypassed for posttranslational protein targeting in chloroplasts. Plant Cell **19:** 1635–1648.

Viana, A.A., Li, M., and Schnell, D.J. (2010). Determinants for stop-transfer and post-import pathways for protein targeting to the chloroplast inner envelope membrane. J. Biol. Chem. **285:** 12948–12960.

Vothknecht, U.C., Otters, S., Hennig, R., and Schneider, D. (2012). Vipp1: a very important protein in plastids?! J. Exp. Bot. **63:** 1699–1712.

Walter, B., Hristou, A., Nowaczyk, M.M., and Schünemann, D. (2015). *In vitro* reconstitution of co-translational D1 insertion reveals a role of the cpSec-Alb3 translocase and Vipp1 in photosystem II biogenesis. Biochem. J. **468:** 315–324.

Wang, P., and Dalbey, R.E. (2011). Inserting membrane proteins: the YidC/Oxa1/Alb3 machinery in bacteria, mitochondria, and chloroplasts. Biochim. Biophys. Acta **1808:** 866–875.

Woody, S.T., Austin-Phillips, S., Amasino, R.M., and Krysan, P.J. (2007). The *WiscDsLox* T-DNA collection: an arabidopsis community resource generated by using an improved high-throughput T-DNA sequencing pipeline. J. Plant Res. **120:** 157–165.

Wu, F.H., Shen, S.C., Lee, L.Y., Lee, S.H., Chan, M.T., and Lin, C.S. (2009). Tape-*Arabidopsis* Sandwich - a simpler *Arabidopsis* protoplast isolation method. Plant Methods **5:** 16.

Xia, Z., Broadhurst, R.W., Laue, E.D., Bryant, D.A., Golbeck, J.H., and Bendall, D.S. (1998). Structure and properties in solution of PsaD, an extrinsic polypeptide of photosystem I. Eur. J. Biochem. **255:** 309–316.

Yi, L., and Dalbey, R.E. (2005). Oxa1/Alb3/YidC system for insertion of membrane proteins in mitochondria, chloroplasts and bacteria (review). Mol. Membr. Biol. **22:** 101–111.

Ytterberg, A.J., Peltier, J.B., and van Wijk, K.J. (2006). Protein profiling of plastoglobules in chloroplasts and chromoplasts. A surprising site for differential accumulation of metabolic enzymes. Plant Physiol. **140:** 984–997.

Yu, B., Gruber, M.Y., Khachatourians, G.G., Zhou, R., Epp, D.J., Hegedus, D.D., Parkin, I.A., Welsch, R., and Hannoufa, A. (2012). *Arabidopsis* cpSRP54 regulates carotenoid accumulation in *Arabidopsis* and *Brassica napus.* J. Exp. Bot. **63:** 5189–5202.

Zhang, L., Kato, Y., Otters, S., Vothknecht, U.C., and Sakamoto, W. (2012). Essential role of VIPP1 in chloroplast envelope maintenance in *Arabidopsis.* Plant Cell **24:** 3695–3707.

Zhang, R., Wise, R.R., Struck, K.R., and Sharkey, T.D. (2010). Moderate heat stress of *Arabidopsis thaliana* leaves causes chloroplast swelling and plastoglobule formation. Photosynth. Res. **105:** 123–134.